Active Channel Sparsification for Uplink Massive MIMO with Uniform Planar Array

Han Yu, *Student Member, IEEE*, Li You, *Member, IEEE*,
Wenjin Wang, *Member, IEEE*, and Xinping Yi, *Member, IEEE*

***Abstract*—We consider a single-cell massive multi-input multi-output (MIMO) network with uniform planar array (UPA) antennas equipped at the base station that serves a number of single-antenna users. In the overloaded multi-user setting, it is likely that users' channels are highly spatial-correlated with overlapping spectrum in the angular domain, which imposes challenges on uplink channel estimation and data transmission due to potential pilot contamination during uplink training and multiuser interference during uplink data transmission. To mitigate the effect of multiuser channel spatial correlation, we adopt a recently proposed active channel sparsification strategy, and propose a novel method for joint user and beam selection in the angular domain. In particular, we represent all users' channels in the angular/beam domain, taking advantage of the doubly block Toeplitz structure of the channel covariance matrix for UPA. Accordingly, we construct a weighted bipartite graph to represent the beam and user association for ease of user/beam selection. By doing so, we reformulate the problems of mean square error minimization for uplink channel estimation and sum rate maximization for uplink data detection as two mixed integer linear programs (MILPs), by which the challenging joint user and beam selection problem can be efficiently solved via off-the-shelf MILP solvers. The simulation results demonstrate the effectiveness of our active channel sparsification strategy for the joint user and beam selection.**

***Index Terms*—Massive MIMO, channel estimation, user selection, active channel sparsification.**

I. Introduction

Being a key technology of the fifth generation (5G) and beyond wireless communication systems, massive multi-input multi-output (MIMO) has been, and will be, deployed in many practical network scenarios. Equipped with massive antennas that could be linear, planar or other antenna geometries, the base station is able to serve tens of users simultaneously, offering very high spectral and energy efficiencies [1] [2].

Due to the collocation of a large number of antenna elements, the channels of massive MIMO with uniform linear/planar array (ULA/UPA) exhibit high spatial correlation, provided the limited number of scatters around the antenna array. Aiming to exploit the benefit of spatial correlation in massive MIMO, a number of works in the literature made the assumption of the low-rankness of the channel covariance matrices (e.g., [3]–[5]). Such an assumption has been shown very useful and led to a number of tractable theoretical analysis. The obtained insights from theoretical analysis have guided the practical system design in the past years, although the validation of such assumption is still under debate for sub-6GHz frequency bands.

Under the low rankness assumption, when the user's channel is cast into the angular or beam domain, its angular spectral density exhibits some sparsity property (e.g., [3]–[5]) – most spectral density values are close to zero – with massive antennas. As such, if the users' locations are sufficiently apart with no overlapping on their angle spread regions of their angle-of-arrival (uplink) or angle-of-departure (downlink), their channel subspaces are orthogonal in an asymptotic sense. Such a sparsity property has been demonstrated to be very useful in both time-division duplex (TDD) and frequency-division duplex (FDD) systems. For instance, it has been used for the coordinated design of pilot reuse strategies in TDD mode (e.g., [3], [5]) by avoiding allocating the same pilot to the users with overlapping spectrum in the angular domain. It has been also employed for precoder design and user grouping in FDD mode (e.g., [4], [6]) by designing orthogonal precoders for the users in the same group with high channel spatial correlation.

Since then, exploiting channel sparsity in the beam/angular domain has extensive applications in massive MIMO systems, such as pilot decontamination and channel estimation in TDD massive MIMO [7]–[11], downlink channel estimation in FDD massive MIMO [12]–[16], and spatial multiplexing in mmWave massive MIMO systems [17]–[19], among many others. It is worth noting that most of the approaches rely highly on the assumption of channel sparsity in the angular/beam domain, and require hundreds of antennas in the single dimension to promote channel sparsity. Unfortunately, when it comes to UPA, channel sparsity may not be taken as granted, because each row or column may only have a limited number of antenna elements.

The question then arises as to what if channel sparsity does not hold. Can we still enjoy the benefit of channel sparsity

Manuscript received August 7, 2020; revised January 6, 2021; accepted March 27, 2021. The work of H. Yu and X. Yi was supported in part by the Royal Society International Exchanges Program under award IEC\NSFC\201080. The work of L. You and W. Wang was supported in part by the National Key R&D Program of China under Grant 2019YFB1803102, in part by the National Natural Science Foundation of China under Grants 61801114, 61631018, and 61761136016, in part by the Jiangsu Province Basic Research Project under Grant BK20192002, and in part by the Fundamental Research Funds for the Central Universities.

H. Yu and X. Yi are with the Department of Electrical Engineering and Electronics, University of Liverpool, L69 3BX, United Kingdom. Email: {han.yu, xinping.yi}@liverpool.ac.uk.

L. You, and W. Wang are with the National Mobile Communications Research Laboratory, Southeast University, Nanjing 210096, China, and also with the Purple Mountain Laboratories, Nanjing 211100, China (e-mail: {liyou,wangwj}@seu.edu.cn.

Communicated by M. Kountouris.

by artificially creating such property? The answer is yes. Very recently, a novel concept of active channel sparsification (ACS) has been proposed in [20] for FDD massive MIMO with ULA, in order to reduce the feedback overhead with negligible system performance degradation. In contrast to conventional wisdom, ACS does not rely on the assumption of channel sparsity, and can adapt to any level of possible channel sparsity (if any) through active sparsification. The main idea is to 1) represent each user's channel by the weighted sum of a set of common bases vectors (i.e., virtual beams), for which the columns of discrete Fourier transform (DFT) matrix are usually used for ULA; 2) construct a weighted bipartite graph to describe channel representation by establishing the user-beam association with respect to the weighted combinations; and finally 3) switch on/off beams to avoid beam overlapping among different users and at the same time to achieve the maximum multiplexing gain. The key enabler is to bridge the multiplexing gain (i.e., prelog of the sum rate expression) to the maximum cardinality bipartite matching of the graph representation. Taking advantage of combinatorial optimization tools, maximizing multiplexing gain problem is translated to an MILP, for which the off-the-shelf solvers can find a feasible beam/user selection in an effective way. Since then, such an ACS concept had been adopted in a number of scenarios. For instance, it has been applied to dual-polarized FDD massive MIMO systems for the design of sparsifying precoders in [21].

In this paper, we revisit such an ACS concept and apply it to the joint design of the uplink massive MIMO with UPA, by taking into account both channel estimation and data transmission. Due to channel spatial correlation, the users' channels are overlapping in the beam domain with high probability, when a large number of users are requesting service simultaneously, which results in severe pilot contamination for uplink training and multiuser interference for uplink transmission. To resolve these issues, we adopt the ACS strategy by switching on/off beams and scheduling users to *artificially* make the overall users' effective channels as sparse as possible without degrading too much channel estimation accuracy as well as uplink sum rate performance. Compared with the existing pilot decontamination methods, e.g., [3], [22]–[24], the proposed approach does not rely on the assumption of channel sparsity, and takes both uplink channel estimation and data transmission into account. On the other hand, our approach improves the original formulation in [20] by considering both performance metrics in the infinite SNR (i.e., multiplexing gain) and finite SNR (i.e., signal-to-interference-plus-noise ratio) regimes, as well as explicit user selection. Specifically, our contributions in this paper are three-fold.

- By analyzing the channel covariance matrix of UPA massive MIMO, which has a doubly block Toeplitz structure, we approximately represent users' channel in the angular/beam domain by employing the two-dimensional DFT basis vectors as virtual beams. As such, we formally confirm in a principled way that if the representing beams of different users are not overlapping, then the same pilot can be reused for channel estimation of these users without pilot contamination. This agrees with the well-known results for ULA massive MIMO.
- We explicitly implement the ACS strategy by introducing a set of binary variables for the selection of beams and users, by which we construct the effective channel covariance matrices by projecting the original ones onto the subspace spanned by the selected virtual beams. Such projected covariance matrices serve for channel estimation and uplink receiver design. It will be shown effective by simulations with respect to sum rate and channel estimation performance even in the non-asymptotic regime with a finite number of antennas.
- By representing the beam-user association as a weighted bipartite graph, the joint beam and user selection problem can be cast as a maximum cardinality bipartite matching problem on the graph representation. By doing so, we reformulate the mean squared error (MSE) minimization and sum rate maximization problems as two MILPs, for which off-the-shelf solvers yield feasible solutions. To further mitigate the limitations of parameter choosing, we propose an alternating projection algorithm between two MILPs.

Numerical results are also provided to demonstrate the effectiveness of our proposed methods in both rectangular (16×8) UPA and ULA (128×1) antenna configurations. Notably, our proposed uplink channel estimation and transmission methods with joint beam and user selection have superior sum rate and MSE performance than the vanilla minimum mean squared error (MMSE) scheme without user/beam selection as well as the classical baselines with user grouping.

The rest of this paper is organized as follows. In Section II, we present the massive MIMO system model with uplink channel training and data transmission, followed by asymptotic analysis on the channel covariance matrix and the ACS framework in Section III. We propose in Section IV a joint beam and user selection approach based on a weighted bipartite graph representation. The simulation results and the conclusion are presented in Sections V and VI, respectively.

Notation: We use x, $\boldsymbol{x}$, and $\boldsymbol{X}$ to represent scalar, vector, and matrix, respectively. Specifically, $[\boldsymbol{x}]_i$ denotes the i-th entry of vector $\boldsymbol{x}$. $[\boldsymbol{X}]_{i,j}$ denotes the element in the i-th row and j-th column of matrix $\boldsymbol{X}$. $\{\boldsymbol{x}_n\}_{n=1}^N \triangleq \{\boldsymbol{x}_1, \boldsymbol{x}_2, \ldots, \boldsymbol{x}_N\}$. For two integers M and N with $M < N$, $[N] \triangleq \{1, 2, \ldots, N\}$ and $[M, N] \triangleq \{M, M+1, \ldots, N\}$. $\boldsymbol{X}^{\mathsf{T}}$, $\boldsymbol{X}^{\mathsf{H}}$ and $\boldsymbol{X}^{\dagger}$ denote the transpose, conjugate transpose and Moor-Penros pseudoinverse of a matrix $\boldsymbol{X}$, respectively. $\boldsymbol{X}$ is Hermitian if and only if $\boldsymbol{X} = \boldsymbol{X}^{\mathsf{H}}$. $\mathrm{tr}(\boldsymbol{X})$ denotes the trace of a matrix $\boldsymbol{X}$. $\|\boldsymbol{x}\|$ denotes the ℓ_2 norm of a vector $\boldsymbol{x}$. $\mathbb{E}\{\cdot\}$ denotes the expectation. The Kronecker product of two matrices $\boldsymbol{X}$ and $\boldsymbol{Y}$ is denoted by $\boldsymbol{X} \otimes \boldsymbol{Y}$. $\mathrm{vec}(\boldsymbol{X})$ is the column vectorization of the matrix $\boldsymbol{X}$. $\mathrm{diag}\left(\{x_1, \ldots, x_N\}\right)$ denotes the diagonal matrix with $x_1, \ldots, x_N$ at the main diagonal. $x = \max_p\{\boldsymbol{a}\}$ means x is the sum of the largest p elements in the vector $\boldsymbol{a}$. $\mathcal{N}_{\mathbb{C}}(\alpha, \beta)$ denotes the complex normal distribution, where α and β are mean (vector) and variance (matrix), respectively.

An $n \times n$ matrix $\boldsymbol{X}$ has a Toeplitz structure if and only if $[\boldsymbol{X}]_{i,j} = [\boldsymbol{X}]_{i+1,j+1}$ for any $i \in [n]$ and $j \in [n]$. An $mn \times mn$ matrix $\boldsymbol{X}$ is a doubly block Toeplitz matrix, if $\boldsymbol{X}$

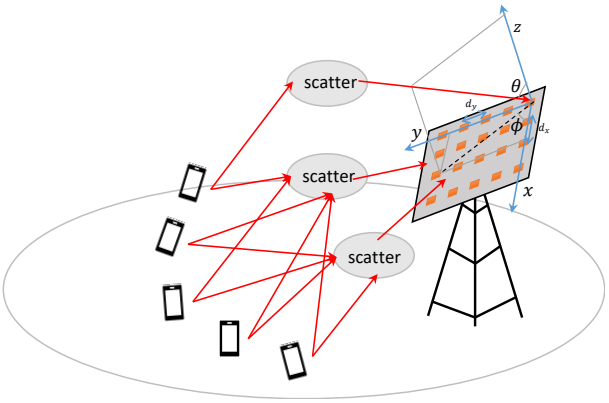

Fig. 1: A single-cell multi-user massive MIMO network with UPA antennas equipped at the base station that server a number of single-antenna users.

has a Toeplitz structure with $m \times m$ blocks and each block also has a Toeplitz structure with size $n \times n$, i.e., $[[\boldsymbol{X}]_{i,j}]_{p,q} = [[\boldsymbol{X}]_{i+1,j+1}]_{p+1,q+1}$ for $i, j \in [m]$ and $p, q \in [n]$. $\boldsymbol{I}_M$ is the $M \times M$ identity matrix, and $\boldsymbol{V}_M$ is the DFT matrices with $[\boldsymbol{V}_M]_{p,q} = \frac{1}{\sqrt{M}} e^{-\jmath \frac{2\pi(p-1)(q-1)}{M}}$ for all $p \in [M], q \in [M]$.

II. System Model

A. Channel Model

We consider a single-cell uplink massive MIMO system with the base station equipped with an $M_x \times M_y$ UPA serving N_U single-antenna users. Let $M = M_x \times M_y$ be the total number of antenna elements. Given the angle intervals of azimuth $\mathcal{A}$ and elevation $\mathcal{B}$, the uplink channel vector can be given by [5], [20]

$$\boldsymbol{h} = \int_{\mathcal{B}} \int_{\mathcal{A}} \beta(\theta, \phi) \boldsymbol{a}(\theta, \phi) d\theta d\phi \tag{1}$$

where $\mathcal{A} = [\theta_{\min}, \theta_{\max}]$, $\mathcal{B} = [\phi_{\min}, \phi_{\max}]$ and $|\mathcal{A}| = 2\delta_\theta$ and $|\mathcal{B}| = 2\delta_\phi$. Note that δ_θ and δ_ϕ are the angular spread (AS) of azimuth and elevation, respectively. The complex gain $\beta(\theta, \phi)$ is assumed to be independent and identically distributed (i.i.d.) across paths, with constant second-order statistics, i.e., $\beta \triangleq \mathbb{E}\{|\beta(\theta, \phi)|^2\}$, and $\boldsymbol{a}(\theta, \phi) \in \mathbb{C}^{M \times 1}$ is the steering vector of UPA and can be written as [25], [26], [27]

$$\begin{aligned} \boldsymbol{a}(\theta, \phi) &= \boldsymbol{a}_y(\theta, \phi) \otimes \boldsymbol{a}_x(\theta, \phi) \\ &= \begin{bmatrix} 1 \\ e^{\jmath \frac{2\pi d_y}{\lambda_w} \sin(\phi)\sin(\theta)} \\ \vdots \\ e^{\jmath \frac{2\pi d_y (M_y - 1)}{\lambda_w} \sin(\phi)\sin(\theta)} \end{bmatrix} \otimes \begin{bmatrix} 1 \\ e^{\jmath \frac{2\pi d_x}{\lambda_w} \sin(\phi)\cos(\theta)} \\ \vdots \\ e^{\jmath \frac{2\pi d_x (M_x - 1)}{\lambda_w} \sin(\phi)\cos(\theta)} \end{bmatrix} \end{aligned} \tag{2}$$

where d_x and d_y are antenna spacing of column and row arrays, respectively (see Fig. 1), and λ_w is the wavelength.

B. Uplink Channel Estimation

During the uplink training phase, the received pilot signal at the base station is expressed as

$$\boldsymbol{Y} = \boldsymbol{h}_i \boldsymbol{s}_i^{\mathsf{T}} + \sum_{j \neq i} \boldsymbol{h}_j \boldsymbol{s}_j^{\mathsf{T}} + \boldsymbol{N} \tag{3}$$

where $\boldsymbol{s}_i$ is the pilot sequence assigned to user i with $\boldsymbol{s}_i = [s_{i1}, s_{i2}, \cdots, s_{i\tau}]^{\mathsf{T}}$. The pilot sequences are assumed orthogonal, i.e., $\boldsymbol{s}_i^{\mathsf{H}} \boldsymbol{s}_j = \tau$ if $i = j$ and 0 otherwise, where τ is the length of pilot sequences. $\boldsymbol{N} \in \mathbb{C}^{M \times \tau}$ is additive white Gaussian noise (AWGN) at the antennas across pilot dimensions, where each element is i.i.d. Gaussian with zero mean and variance σ^2. The uplink channel $\boldsymbol{h}_i \in \mathbb{C}^{M \times 1} \sim \mathcal{N}_{\mathbb{C}}(\boldsymbol{0}, \boldsymbol{R}_i)$ of user i is given in a similar form in (1) where $\boldsymbol{R}_i = \mathbb{E}\{\boldsymbol{h}_i \boldsymbol{h}_i^{\mathsf{H}}\}$ is the channel covariance matrix.

For clarity, we only take into account the interference caused by the users with the same pilot sequence, while the interference from the users assigned with different pilot sequences can be easily mitigated by multiplying the pilot sequence. Thus, let all users of interest send the same pilot signal $\boldsymbol{s}_i = \boldsymbol{s}$ for all i. Before proceeding further, we recall the MMSE channel estimation. Let $\boldsymbol{S} = \boldsymbol{s} \otimes \boldsymbol{I}_M$ with $\boldsymbol{S}^{\mathsf{H}} \boldsymbol{S} = \tau \boldsymbol{I}_M$. By vectorization [3], we represent the received pilot signal in (3) as $\boldsymbol{y} = \boldsymbol{S} \sum_{i=1}^{N_U} \boldsymbol{h}_i + \boldsymbol{n}$, where $\boldsymbol{y} = \mathrm{vec}(\boldsymbol{Y})$ and $\boldsymbol{n} = \mathrm{vec}(\boldsymbol{N})$. Hence, the linear MMSE estimator for a desired channel $\boldsymbol{h}_i$ can be given by

$$\hat{\boldsymbol{h}}_i^{\mathrm{MMSE}} = \boldsymbol{R}_i \left(\sigma^2 \boldsymbol{I}_M + \tau \sum_{i=1}^{N_U} \boldsymbol{R}_i \right)^{-1} \boldsymbol{S}^{\mathsf{H}} \boldsymbol{y}. \tag{4}$$

C. Uplink Data Transmission

During the uplink data transmission phase, the received signal at the BS can be written as

$$\boldsymbol{y}^d = \sum_{i=1}^{N_U} \boldsymbol{h}_i x_i^d + \boldsymbol{n}^d \tag{5}$$

where x_i^d is the transmitted signal from the i-th user, $\boldsymbol{y}^d \in \mathbb{C}^{M \times 1}$ is the overall received signal at the base station, and each element of $\boldsymbol{n}^d \in \mathbb{C}^{M \times 1}$ is the i.i.d. Gaussian noise. In this phase, linear receive beamformers $\boldsymbol{w}_i \in \mathbb{C}^{M \times 1}$ are designed based on the estimated channels in the training phase to recover the transmitted signal x_i^d, that is, $\hat{x}_i^d = \boldsymbol{w}_i^{\mathsf{H}} \boldsymbol{y}^d$.

Due to the overlapping of channel spectrum in the angular domain, the overloaded multiuser system incurs potential pilot contamination and interference-limited data transmission. A natural way is to select a subset of users to access the channel resource simultaneously. In view of the fact that users' channels in the beam domain have some nice properties (e.g., sparsity), we perform user selection in the beam domain, taking possible beam selection into account. Our goal is to design proper uplink channel estimators and receiving beamformers at the base station with joint beam and user selection, striking a balance between pilot decontamination and data transmission. Before proceeding further, we analyze the asymptotic behavior of the channel covariance matrix, which will guide our design of channel estimation and joint beam/user selection.

III. Active Channel Sparsification and Asymptotic Analysis

For the asymptotic analysis of massive MIMO with UPA antennas, we start with the following theorem, which has been widely-accepted in the literature yet not formally proved.

Theorem 1. *For the UPA massive MIMO, the channel covariance matrix $\boldsymbol{R}=\mathbb{E}\{\boldsymbol{h}\boldsymbol{h}^{\mathsf{H}}\}$ has a Hermitian doubly block Toeplitz structure, so that it can be asymptotically diagonalized by the 2D-DFT matrix, i.e.,*

$$\lim_{M_x,M_y\to\infty}\boldsymbol{R}=(\boldsymbol{V}_{M_y}\otimes\boldsymbol{V}_{M_x})\boldsymbol{\Lambda}(\boldsymbol{V}_{M_y}\otimes\boldsymbol{V}_{M_x})^{\mathsf{H}} \tag{6}$$

$$=\sum_{a=1}^{M_y}\sum_{b=1}^{M_x}\chi(\omega_a,\zeta_b)(\boldsymbol{f}_a\otimes\boldsymbol{g}_b)(\boldsymbol{f}_a\otimes\boldsymbol{g}_b)^{\mathsf{H}} \tag{7}$$

where $\{\boldsymbol{f}_a\}_{a=1}^{M_y}$ and $\{\boldsymbol{g}_b\}_{b=1}^{M_x}$ are columns of the DFT matrices, and $\boldsymbol{\Lambda}\in\mathbb{C}^{M\times M}$ is a diagonal matrix with the $((a-1)M_y+b)$-th diagonal element being

$$\chi(\omega_a,\zeta_b)=\sum_{\mu}\sum_{\nu}r_{\mu,\nu}e^{\jmath 2\pi(\mu\omega_a+\nu\zeta_b)} \tag{8}$$

for which $(\omega_a,\zeta_b)=(\frac{a-1}{2M_y},\frac{b-1}{2M_x})$ and

$$r_{\mu,\nu}=\beta\int_{\mathcal{B}}\int_{\mathcal{A}}e^{-\jmath\frac{2\pi}{\lambda_w}(d_x\nu+d_y\mu)\sin\phi\sin\theta}d\theta d\phi \tag{9}$$

with $\mu\in[-M_y,M_y]$, $\nu\in[-M_x,M_x]$, and $\beta=\mathbb{E}\{|\beta(\theta,\phi)|^2\}$.

Proof. See Appendix A. □

Remark 1. *Theorem 1 guarantees that the covariance matrix of UPA massive MIMO channel can be asymptotically represented by the linear combination of a set of common basis vectors coming from 2D-DFT matrices. This is a generalized version of the covariance matrix in ULA massive MIMO from Toeplitz to doubly block Toeplitz. When $M_x=1$ or $M_y=1$, Theorem 1 reduces to the ULA setting with the channel covariance matrix being Toeplitz and the common basis vectors being from 1D DFT matrix, which agrees with that in [4].*

In what follows, Theorem 1 will be shown useful for channel representation, which is the key enabler of joint user and beam selection in Section IV. As ULA is a special case of UPA, we focus on UPA hereafter, and the ULA setting can be easily specified.

For $m\in[M]$, denote by $\boldsymbol{v}_m=\boldsymbol{f}_a\otimes\boldsymbol{g}_b$ with $m=(a-1)M_y+b$, and $\boldsymbol{V}=\boldsymbol{V}_{M_y}\otimes\boldsymbol{V}_{M_x}$. By Karhunen-Loève transform, the channel vector can be asymptotically represented as

$$\boldsymbol{h}_{i,\infty}=\boldsymbol{V}\boldsymbol{\Lambda}_i^{\frac{1}{2}}\boldsymbol{h}_w=\sum_{m=1}^{M}\sqrt{\lambda_{i,m}}h_m\boldsymbol{v}_m \tag{10}$$

where h_m is the m-th entry of $\boldsymbol{h}_w\sim\mathcal{N}_{\mathbb{C}}(\boldsymbol{0},\mathbf{I})$, and $\lambda_{i,m}$ is the m-th diagonal element of $\boldsymbol{\Lambda}_i$.

For brevity, we let $\tau=1$ and $s=1$. Thus, the MMSE channel estimate turns to be

$$\hat{\boldsymbol{h}}_i^{\text{MMSE}}=\boldsymbol{R}_i\left(\sigma^2\boldsymbol{I}_M+\sum_{j=1}^{N_U}\boldsymbol{R}_j\right)^{-1}\boldsymbol{y} \tag{11}$$

which asymptotically approaches to

$$\hat{\boldsymbol{h}}_{i,\infty}^{\text{MMSE}}=\sum_{m=1}^{M}\frac{\lambda_{i,m}}{\sum_{j=1}^{N_U}\lambda_{j,m}+\sigma^2}\boldsymbol{v}_m\boldsymbol{v}_m^{\mathsf{H}}\boldsymbol{y} \tag{12}$$

with $\boldsymbol{y}=\sum_j\boldsymbol{h}_j+\boldsymbol{n}$ being the training phase signal when pilot $s=1$.

Theorem 2. *Let $\mathcal{S}_i=\{m:\lambda_{i,m}>0\}$ be the support of beam representation of user i's channel. If $\mathcal{S}_i\cap\mathcal{S}_j=\emptyset$ for all $j\neq i$, then $\text{MSE}_{i,\infty}=0$ when SNR tends to infinity.*

Proof. From (12), the asymptotic MSE can be given by

$$\text{MSE}_{i,\infty}=\mathbb{E}\left\{\|\boldsymbol{h}_{i,\infty}-\hat{\boldsymbol{h}}_{i,\infty}^{\text{MMSE}}\|^2\right\} \tag{13}$$

$$=\text{tr}\left(\sum_{m=1}^{M}\lambda_{i,m}\left(1-\frac{\lambda_{i,m}}{\sum_{j=1}^{N_U}\lambda_{j,m}+\sigma^2}\right)\boldsymbol{v}_m\boldsymbol{v}_m^{\mathsf{H}}\right) \tag{14}$$

$$=\sum_{m=1}^{M}\lambda_{i,m}\left(1-\frac{\lambda_{i,m}}{\sum_{j=1}^{N_U}\lambda_{j,m}+\sigma^2}\right) \tag{15}$$

where (14) is due to $\text{tr}(\boldsymbol{v}_m\boldsymbol{v}_m^{\mathsf{H}})=\text{tr}(\boldsymbol{v}_m^{\mathsf{H}}\boldsymbol{v}_m)=1$.

In the high SNR regime, i.e., $\sigma^2\to0$, $\text{MSE}_{i,\infty}$ in (15) approaches

$$\lim_{\sigma^2\to0}\text{MSE}_{i,\infty}=\sum_{m=1}^{M}\left(\lambda_{i,m}-\frac{\lambda_{i,m}^2}{\sum_{j=1}^{N_U}\lambda_{j,m}}\right)$$

$$=\sum_{m=1}^{M}\left(\frac{\sum_{j=1}^{N_U}\lambda_{i,m}\lambda_{j,m}-\lambda_{i,m}^2}{\sum_{j=1}^{N_U}\lambda_{j,m}}\right) \tag{16}$$

$$=\sum_{m=1}^{M}\left(\frac{\sum_{j\neq i}^{N_U}\lambda_{i,m}\lambda_{j,m}}{\sum_{j=1}^{N_U}\lambda_{j,m}}\right)=0 \tag{17}$$

where the last equation is due to the fact that $\mathcal{S}_i\cap\mathcal{S}_j=\emptyset$ implies $\lambda_{i,m}\lambda_{j,m}=0$ for any $m\in[M]$ when $i\neq j$. This proves Theorem 2. □

Theorem 2 agrees with the existing results for ULA in [3], [5] that, if users have non-overlapping spectrum in the beam domain, they can be assigned with the same pilot without causing pilot contamination. Inspired by this, one may image that if the overlapping beams among users can be controlled by user and/or beam selection, pilot contamination can be manually mitigated even if users have overlapping spectrum. This motivates the ACS strategy.

A. Active Channel Sparsification

For user/beam selection, we introduce two sets of binary variables $\{x_m\}_{m=1}^{M}$ and $\{y_i\}_{i=1}^{N_U}$ as designing parameters to control the activity of beams and users, respectively, as follows

$$x_m=\begin{cases}1, & \text{virtual beam } m \text{ is selected,}\\ 0, & \text{otherwise.}\end{cases} \tag{18}$$

$$y_i=\begin{cases}1, & \text{user } i \text{ is selected,}\\ 0, & \text{otherwise.}\end{cases} \tag{19}$$

where $m=(a-1)M_y+b$ is the index of the virtual beam corresponding to the antenna at a-th column and b-th row in the UPA setting.

As in (10), the channel vector can be asymptotically represented by a linear combination of 2D-DFT beams, so that channel estimation is to figure out the coefficients of the linear combination. To avoid pilot contamination, a subset of users is selected to reuse the same pilot, whilst it may not be necessary to estimate all coefficients of the linear combination.

1) Channel Estimation: With beam selection enabled, we construct an effective channel covariance matrix for user i, which can be represented by

$$\boldsymbol{R}_i^{\text{ON/OFF}} = \sum_{m=1}^{M} x_m \boldsymbol{v}_m \boldsymbol{v}_m^{\mathsf{H}} \boldsymbol{R}_i. \tag{20}$$

When $x_m = 1$ for all $m \in [M]$, $\boldsymbol{R}_i^{\text{ON/OFF}}$ reduces to the original $\boldsymbol{R}_i$, where "ON/OFF" indicates the beam and user selection through the binary variables $\{x_m\}_{m=1}^{M}$ and $\{y_i\}_{i=1}^{N_U}$. Such a covariance matrix can be interpreted as the projection of the original covariance matrix $\boldsymbol{R}_i$ onto the subspace spanned by the set of selected beams $\{\boldsymbol{v}_m : x_m = 1\}_{m=1}^{M}$. When $M_x, M_y \to \infty$, $\boldsymbol{R}_i^{\text{ON/OFF}}$ can be further represented in the following way

$$\lim_{M_x, M_y \to \infty} \boldsymbol{R}_i^{\text{ON/OFF}} = \boldsymbol{V}\boldsymbol{X}\boldsymbol{V}^{\mathsf{H}}\boldsymbol{R}_i\boldsymbol{V}\boldsymbol{V}^{\mathsf{H}} = \boldsymbol{V}(\boldsymbol{X}\boldsymbol{\Lambda}_i)\boldsymbol{V}^{\mathsf{H}} \tag{21}$$

$$= \sum_{m=1}^{M} \lambda_{i,m} x_m \boldsymbol{v}_m \boldsymbol{v}_m^{\mathsf{H}} \tag{22}$$

where $\lambda_{i,m}$ is the m-th diagonal element of $\boldsymbol{\Lambda}_i$ defined in Theorem 1 for user i, and $\boldsymbol{X} = \text{diag}(x_1, \ldots, x_M)$. It looks as if some virtual beams are selected to asymptotically represent the channel covariance matrices.

Plugging (20) into (11), we obtain the channel estimate $\hat{\boldsymbol{h}}_i^{\text{ON/OFF}}$ of user i by beam selection,

$$\hat{\boldsymbol{h}}_i^{\text{ON/OFF}} = \boldsymbol{R}_i^{\text{ON/OFF}} \left(\sigma^2 \boldsymbol{I}_M + \sum_{j=1}^{N_U} y_j \boldsymbol{R}_j^{\text{ON/OFF}} \right)^{-1} \boldsymbol{y} \tag{23}$$

which asymptotically approaches $\hat{\boldsymbol{h}}_{i,\infty}^{\text{ON/OFF}}$ as $M_x, M_y \to \infty$, defined as

$$\hat{\boldsymbol{h}}_{i,\infty}^{\text{ON/OFF}} = \sum_{m=1}^{M} \frac{\lambda_{i,m} x_m}{\sum_{j=1}^{N_U} \lambda_{j,m} y_j x_m + \sigma^2} \boldsymbol{v}_m \boldsymbol{v}_m^{\mathsf{H}} \boldsymbol{y} \tag{24}$$

$$= \sum_{m=1}^{M} \frac{w_m \lambda_{i,m} x_m}{\sum_{j=1}^{N_U} \lambda_{j,m} y_j x_m + \sigma^2} \boldsymbol{v}_m \tag{25}$$

with $w_m = \boldsymbol{v}_m^{\mathsf{H}} \boldsymbol{y}$. It looks as if the channel estimator is a linear combination of the selected beams in an asymptotic sense.

Thus, the asymptotic MSE of channel estimation with beam selection can be given by

$$\text{MSE}_{i,\infty}^{\text{ON/OFF}} = \mathbb{E}\left\{ \|\boldsymbol{h}_{i,\infty} - \hat{\boldsymbol{h}}_{i,\infty}^{\text{ON/OFF}}\|^2 \right\} \tag{26}$$

$$= \sum_{m=1}^{M} \lambda_{i,m} \left(1 - \frac{\lambda_{i,m} x_m}{\sum_{j=1}^{N_U} \lambda_{j,m} y_j x_m + \sigma^2} \right). \tag{27}$$

Note that if no user or beam selection is applied, i.e., $x_m = y_j = 1$ for all $m \in [M]$ and $j \in [N_U]$, then (27) boils down to (15).

2) Data Transmission: For simplicity, we adopt the zero-forcing (ZF) beamforming at the base station, which is designed based on uplink channel estimates, that is,

$$\boldsymbol{w}_i^{\text{ON/OFF}} \in \mathcal{R}\{\hat{\boldsymbol{h}}_i^{\text{ON/OFF}}\} \cap \mathcal{N}\{\hat{\boldsymbol{h}}_j^{\text{ON/OFF}} : y_j = 1, j \neq i\} \tag{28}$$

where $\mathcal{R}(\cdot)$ and $\mathcal{N}(\cdot)$ are the range and null space of the subspace spanned by the vectors, respectively.

As $M_x, M_y \to \infty$, the ZF beamforming vector asymptotically lies in the subspace spanned by the unselected and the unoccupied beams, i.e.,

$$\boldsymbol{w}_{i,\infty}^{\text{ON/OFF}} \in \text{span}\{\boldsymbol{v}_m : m \in \mathcal{S}\} \tag{29}$$

where $\mathcal{S} = \{m : x_m \lambda_{i,m} > 0 \text{ and } y_j \lambda_{j,m} = 0, \forall j \neq i\}$. Note that $x_m \lambda_{i,m} > 0$ ensures that beam m is active ($x_m = 1$) to represent user i's channel where the corresponding component of $\boldsymbol{v}_m$ has nontrivial contribution ($\lambda_{i,m} > 0$) to the channel representation. In addition, $y_j \lambda_{j,m} = 0, i \neq j$ guarantees that, if user j is active ($y_j = 1$), then it should not cause interference at beam m through $\lambda_{j,m}$; otherwise it should be inactive ($y_j = 0$). Thus, the asymptotic signal-to-interference-plus-noise ratio (SINR) is given by

$$\gamma_{i,\infty} = \frac{\sum_{m=1}^{M} \lambda_{i,m} x_m}{\sum_{j \neq i} \sum_{m=1}^{M} y_j \lambda_{j,m} x_m + \sigma^2} \tag{30}$$

and therefore the corresponding asymptotic rate can be written as $R_{i,\infty} = \log(1 + \gamma_{i,\infty})$.

IV. Joint User and Beam Selection

It is shown from the above asymptotic analysis that beam and user selection has an influence on channel estimation quality and uplink data rate. Our objective of joint channel estimation and data detection can be formulated as the following multi-objective optimization problem:

$$\max \sum_{i=1}^{N_U} y_i R_{i,\infty}, \qquad \min \sum_{i=1}^{N_U} y_i \text{MSE}_{i,\infty}^{\text{ON/OFF}} \tag{31}$$

where the asymptotic quantities are used as the objective functions to guide joint beam and user selection. The performance will be verified by simulation in practical scenarios.

This multi-objective optimization problem can be divided into two sub-problems, so that the tradeoff between two criteria can be made by the following alternating optimization [28]

$$(\mathcal{P}_1): \quad \begin{aligned} &\max \quad \textstyle\sum_{i=1}^{N_U} y_i R_{i,\infty} \\ &\text{s.t.} \quad y_i \text{MSE}_{i,\infty}^{\text{ON/OFF}} \leq P_i, \quad \forall i \in [N_U] \end{aligned} \tag{32}$$

$$(\mathcal{P}_2): \quad \begin{aligned} &\min \quad \textstyle\sum_{i=1}^{N_U} y_i \text{MSE}_{i,\infty}^{\text{ON/OFF}} \\ &\text{s.t.} \quad R_{i,\infty} \geq y_i Q_i, \quad \forall i \in [N_U] \end{aligned} \tag{33}$$

where P_i is the maximum MSE that the i-th user should not exceed if selected to guarantee certain channel estimation accuracy, Q_i is the minimum rate that the i-th user should surpass if selected to guarantee certain quality of service (QoS). Note that if user i is not selected, i.e., $y_i = 0$, then the MSE and rate constraints are automatically satisfied.

In Section IV-D, we employ an alternating projection method to jointly optimize $(\mathcal{P}_1)$ and $(\mathcal{P}_2)$ without relying too much on the threshold parameters $\{P_i\}_{i=1}^{N_U}$ and $\{Q_i\}_{i=1}^{N_U}$.

A. Bipartite Graph Representation

To better illustrate the use of ACS for joint user and beam selection, we represent the users' channels with respect to beams in a bipartite graph $\mathcal{G}$. Let $\mathcal{G} = (\mathcal{B}, \mathcal{U}, \mathcal{E})$ be a bipartite graph, with beams $b \in \mathcal{B}$ on one side and users $u \in \mathcal{U}$ on the other side. Let us introduce another set of binary variables

such that $a_{i,m}=1$ if $\lambda_{i,m}>\delta$ and 0 otherwise, where a small value of $\lambda_{i,m}$ indicates the negligible contribution of the beam m to the i-th user's channel, and δ is a tunable parameter with $\delta=0$ for asymptotic case and a properly chosen positive value to adapt the scenarios with a finite number of antennas. Therefore, a beam b_m and a user u_i are connected with an edge $(b_m,u_i)\in\mathcal{E}$ if $a_{i,m}=1$.

According to the asymptotic channel representation (10), for the user u_i, the channel can be approximately represented as

$$\boldsymbol{h}_i \approx \sum_{b_m\in\mathcal{N}(b)} w_{i,m}\boldsymbol{v}_m \tag{34}$$

where $w_{i,m}=\sqrt{\lambda_{i,m}}h_m$ and $\mathcal{N}(b)=\{b_m\in\mathcal{B}: a_{i,m}=1\}$. Such an approximate channel representation captures the strong beams when $\lambda_{i,m}$ is greater than a certain threshold δ.

Let us explain the impact of beam and user selection on channel estimation and uplink data transmission. It can be observed in Fig. 2 that all users suffer from severe pilot contamination caused by beam overlapping. Basically, four users should be assigned different orthogonal pilots because of the overlapped beam between any two users. Nevertheless, if we actively switch off the beam b_5 and users u_2 and u_3, then the partial channel representations of users 1 and 4 are not overlapping any more, for which the assignment of the same pilot would not cause pilot contamination. Note here that the original channels $\boldsymbol{h}_1$ and $\boldsymbol{h}_4$ are partially represented by beams without b_5. This will not result in issues as long as the partial channel estimation is sufficient to achieve acceptable uplink transmission rate. Therefore, the maximization of uplink transmission rate with beam and user selection will also come to play. Given a proper beam and user selection strategy, only partial channel has been estimated, built on which the receiver beamformers are designed. From the uplink data rate viewpoint, it is prone to more users and possibly fewer beams to remove overlap, while for channel estimation, fewer users with possibly more beams are preferred to reach less pilot contamination and thus higher estimation accuracy. To this end, the joint optimization problem aims to strike a good balance between them.

B. Sum Rate Maximization $(\mathcal{P}_1)$

We first focus on the rate maximization problem $(\mathcal{P}_1)$ in the infinite number of antenna regime, hoping that the obtained solution could shed light on the practical scenarios.

Noting that the direct maximization of $(\mathcal{P}_1)$ is too complicated, especially when taking user scheduling into account, we turn to a revised version of rate maximization. That is, we split the rate maximization into two parts: one is the multiplexing gain (i.e., the pre-log of the rate expression) maximization and the other one is the SINR constraint. In doing so, users will be selected as many as possible to improve the multiplexing gain, whereas the selected users should satisfy the minimum QoS requirement.

Inspired by the treatment in [20], where the sum rate maximization problem is alternatively done by optimizing the multiplexing gain, we transform $(\mathcal{P}_1)$ into a more tractable problem. As proven in [20], the maximum multiplexing gain is equal to the rank of the effective channel, which can be obtained by a reformulated maximum cardinality matching problem with the bipartite graph representation. We point out that the maximum matching is not on the original bipartite graph, but rather on a subgraph with user and beam selection. Let $\mathcal{G}'=(\mathcal{B}',\mathcal{U}',\mathcal{E}')$ be the selected subgraph of $\mathcal{G}=(\mathcal{B},\mathcal{U},\mathcal{E})$ with $\mathcal{B}'\subseteq\mathcal{B}$, $\mathcal{U}'\subseteq\mathcal{U}$, and $\mathcal{E}'\subseteq\mathcal{E}$.

As such, the optimization problem $(\mathcal{P}_1)$ can be reformulated as follows:

$$(\mathcal{P}_1'): \quad \max \quad |\mathcal{M}(\mathcal{B}',\mathcal{U}')| \tag{35a}$$
$$\text{s.t.} \quad \text{MSE}_{i,\infty}^{\text{ON/OFF}} \le P_i, \quad \forall u_i\in\mathcal{U}' \tag{35b}$$
$$\gamma_{i,\infty}\ge\Gamma_i, \quad \forall u_i\in\mathcal{U}', \tag{35c}$$

where $|\mathcal{M}(\mathcal{B}',\mathcal{U}')|$ is the maximum cardinality bipartite matching number of the selected subgraph $\mathcal{G}'=(\mathcal{B}',\mathcal{U}',\mathcal{E}')$, and the constraints guarantee that the selected users have reasonable SINR for uplink transmission and acceptable MSE for uplink channel estimation. Note that in addition to the objective function considered in [20], we impose the SINR and MSE constraints to ensure that the resulting user and beam selection has a reasonable performance guarantee at finite SNR. While the objective function can be similarly translated as those in [20], the constraints (35b)-(35c) call for different treatment. For ease of presentation, we introduce a binary matrix $\boldsymbol{A}=(a_{i,m})\in\{0,1\}^{N_U\times M}$, which is the adjacency matrix [29] of the $M\times N_U$ bipartite graph $\mathcal{G}$.

Theorem 3. *The optimization problem $(\mathcal{P}_1')$ can be transformed to a mixed integer linear program (MILP), whose solution is feasible for $(\mathcal{P}_1')$, as follows*

$$(\mathcal{P}_1''): \quad \max_{x_m,y_i,z_{i,m}} \sum_{m=1}^{M}\sum_{i=1}^{N_U} z_{i,m} \tag{36a}$$
$$\text{s.t.} \quad x_m \le \sum_{i=1}^{N_U}[\boldsymbol{A}]_{i,m}y_i, \quad \forall b_m\in\mathcal{B}, \tag{36b}$$
$$y_i \le \sum_{m=1}^{M}[\boldsymbol{A}]_{i,m}x_m, \quad \forall u_i\in\mathcal{U}, \tag{36c}$$
$$z_{i,m}\le[\boldsymbol{A}]_{i,m}, \quad \forall u_i\in\mathcal{U},\ b_m\in\mathcal{B}, \tag{36d}$$
$$\sum_{i=1}^{N_U} z_{i,m}\le x_m, \quad \forall b_m\in\mathcal{B}, \tag{36e}$$
$$\sum_{m=1}^{M} z_{i,m}\le y_i, \quad \forall u_i\in\mathcal{U}, \tag{36f}$$
$$(1-\tau_{\text{th}})\sum_{j=1}^{N_U} y_j\lambda_{j,m}\le x_m\lambda_{i,m}+c_1(1-x_m)+c_2(1-y_i), \quad \forall u_i\in\mathcal{U},\ b_m\in\mathcal{B}, \tag{36g}$$
$$y_i\tau\sum_{m=1}^{M}\lambda_{i,m}\le\sum_{m=1}^{M}\lambda_{i,m}x_m, \quad \forall u_i\in\mathcal{U}, \tag{36h}$$
$$\sum_{i=1}^{N_U} y_i\lambda_{i,m}\le x_m\tau_\omega^m, \quad \forall b_m\in\mathcal{B}, \tag{36i}$$
$$x_m,y_i\in\{0,1\}, \quad \forall u_i\in\mathcal{U},\ b_m\in\mathcal{B}, \tag{36j}$$
$$z_{i,m}\in[0,1], \quad \forall u_i\in\mathcal{U},\ b_m\in\mathcal{B}, \tag{36k}$$

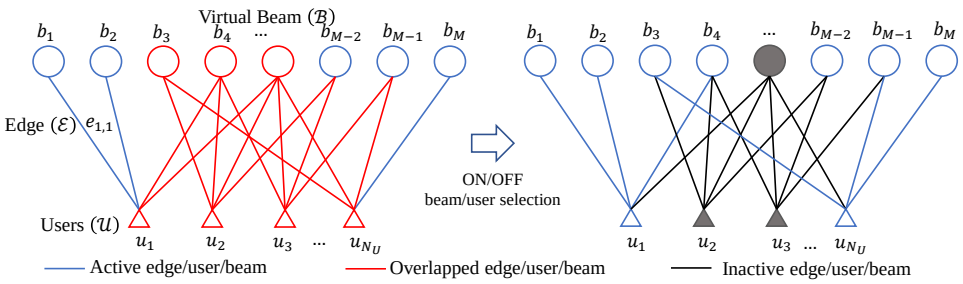

Fig. 2: Weighted bipartite graph representations, where the weight on edges $e_{u,b}$ denotes the coefficient of the linear combination. The figure on the left shows the severe overlapping virtual beams among users, and the one on the right illustrates the non-overlapping virtual beams when ON/OFF user and beam selection is applied.

where the objective function (36a) is translated from the maximum cardinality bipartite matching number in (35a) with $z_{i,m} = 1$ indicating the edge (u_i, b_m) is in the edge set of the maximum matching, and 0 otherwise; the constraints (36b) and (36c) ensure that, if a beam is selected (i.e., $x_m = 1$), there should be a user to occupy it, and vice versa; the constraints (36d), (36e), (36f) are to guarantee the edges $\{(u_i, b_m) : z_{i,m} = 1\}$ in the selected subgraph $\mathcal{G}' = (\mathcal{B}', \mathcal{U}', \mathcal{E}')$ form a maximum cardinality matching; the constraint (36g) is translated from (35b) where $\tau_{\text{th}} \in [0, 1]$ satisfying $\tau_{th} \sum_{m=1}^{M} \lambda_{i,m} = P_i$; and the constraints (36h) and (36i) come from (35c).

Proof. See Appendix B. □

Remark 2. *The hyper-parameters τ_ω^m and $\tau_{\text{th}}, \tau \in [0, 1]$ are designing parameters, and c_1, c_2 are sufficiently large constants. In particular, $\tau_{\text{th}}, \tau \in [0, 1]$ are to control the maximum MSE (36g) and the minimum SINR to guarantee basic QoS, respectively. Note in both (36h) and (36i) that a selected beam-user pair prefers that its power is greater than a certain level of the sum interference seen by the beam. The difference should be attributed to the thresholds τ and τ_{th}. Note also that $z_{i,m}$ is relaxed from $\{0, 1\}$ to $[0, 1]$ to reduce computational complexity. Such a relaxation does not change the solution to $\{z_{i,m}\}$, because with binary-valued x_m and y_i, the polyhedral property of the feasible solution region guarantees that $z_{i,m}$ should be either 0 or 1, so that there is no need to explicitly force $z_{i,m}$ to be binary-valued. This property has been proved in [20]. The solution to $\mathcal{P}_1''$ is also feasible to $\mathcal{P}_1'$ because the constraints in the former are contracted versions of the latter.*

C. MSE Minimization ($\mathcal{P}_2$)

On the other hand, when our main aim is channel estimation accuracy, we can reformulate ($\mathcal{P}_2$) as another optimization problem as follows:

$$(\mathcal{P}_2'): \quad \min \quad \sum_{i=1}^{N_U} \text{MSE}_{i,\infty}^{\text{ON/OFF}} \tag{37a}$$

$$\text{s.t.} \quad \gamma_{i,\infty} \geq \Gamma_i, \quad \forall u_i \in \mathcal{U}', \tag{37b}$$

$$|\mathcal{M}(\mathcal{B}', \mathcal{U}')| \geq U_c^N \tag{37c}$$

where instead of imposing the minimum rate constraint, we impose the multiplexing gain and individual SINR separately. This makes the constraint more tractable.

Theorem 4. *The optimization problem ($\mathcal{P}_2'$) can be transformed to an MILP, whose solution is feasible for ($\mathcal{P}_2'$), as follows*

$$(\mathcal{P}_2''): \quad \min_{x_m, y_i, t_{i,m}} \sum_{m=1}^{M} \sum_{i=1}^{N_U} (y_i \lambda_{i,m} + t_{i,m}) \tag{38a}$$

$$\text{s.t.} \quad y_i \tau \sum_{m=1}^{M} \lambda_{i,m} \leq \sum_{m=1}^{M} \lambda_{i,m} x_m, \quad \forall u_i \in \mathcal{U}, \tag{38b}$$

$$\sum_{i=1}^{N_U} y_i \lambda_{i,m} \leq x_m \tau_\omega^m, \quad \forall b_m \in \mathcal{B}, \tag{38c}$$

$$\sum_{j \neq i} y_j \lambda_{i,m} \lambda_{j,m} \leq \lambda_{i,m} + t_{i,m} + c_3(1 - x_m) + c_4(1 - y_i), \quad \forall u_i \in \mathcal{U}, \ b_m \in \mathcal{B}, \tag{38d}$$

$$\sum_{i=1}^{N_U} y_i \geq U_c^N, \tag{38e}$$

$$x_m, y_i \in \{0, 1\}, \quad \forall b_m \in \mathcal{B}, \ u_i \in \mathcal{U}, \tag{38f}$$

$$t_{i,m} \leq 0, \quad \forall b_m \in \mathcal{B}, \ u_i \in \mathcal{U}, \tag{38g}$$

where the objective function (38a) and the constraint (38d) are translated from (37a); the constraints (38b) and (38c) are from the SINR constraint (37b); the constraint (38e) comes from (37c) to specify the minimum number of active users.

Proof. See Appendix C. □

Remark 3. *The hyper-parameters U_c^N, τ_ω^m, and $\tau \in [0, 1]$ are designing parameters, and c_3, c_4 are sufficiently large constants. The constraint (38c) (see also (36i) in $\mathcal{P}_1''$) is to control the interference-to-noise ratio (INR), and our aim is to keep INR as small as possible. To this end, we should ensure that, given that user i is selected (i.e., $y_i = 1$), if beam m is also selected (i.e., $x_m = 1$), other users $j \neq i$ with significant λ_j are better to be unselected so that the interference from these users to user i on beam m is under certain level. We define $\tau_\omega^m = \max_p\{\lambda_{i,m}, i \in [N_U]\}$ to select the largest p values, and consequently, we only need to give a reasonable value of the integer p rather than an exact threshold to restrict the INR. The solution to $\mathcal{P}_2''$ is also feasible to $\mathcal{P}_2'$ because the constraints in the former are contracted versions of the latter.*

Algorithm 1 Alternating projection

Input: Bipartite graph representation $\mathcal{G}$ constructed with a given δ, its adjacency matrix $\boldsymbol{A}$, the maximum number of iterations $t_{\max}$, and hyper-parameters τ and τ_ω^m
Initialization: FLAG $=1$, $\text{MSE}^0=0$, $\boldsymbol{x}^0=\boldsymbol{x}'^0=(\{x_m\}_{m=1}^M)=\mathbf{0}$, $\boldsymbol{y}^0=(\{y_i\}_{i=1}^{N_U})=\mathbf{0}$
while FLAG **do**
  $t\leftarrow t+1$
  Update τ_{th}^t according to MSE^{t-1}
  Update $\boldsymbol{y}^t$ as the solution of $\{y_i\}$ in $\mathcal{P}_1''$, i.e., (36)
  Update $\boldsymbol{x}^t$ as the solution of $\{x_m\}$ in $\mathcal{P}_1''$, i.e., (36)
  Assign $U_c^N\leftarrow\sum_{i=1}^{N_U}y_i^t$ in $\mathcal{P}_2''$, i.e., (38)
  Update MSE^t as the objective of $\mathcal{P}_2''$, i.e., (38)
  Update $\boldsymbol{x}'^t$ as the solution of $\{x_m\}$ in $\mathcal{P}_2''$, i.e., (38)
  if $\boldsymbol{x}^t=\boldsymbol{x}'^t$ or $t\geq t_{\max}$ **then**
    FLAG $=0$
  end if
end while
Output: $\boldsymbol{x}^t$, $\boldsymbol{y}^t$

D. Joint Optimization via Alternating Projection

It has been shown that the original multi-objective optimization problem (31) can be divided into two sub-problems, so that each sub-problem can be reformulated as an MILP and solved separately, as shown in Sections IV-B and IV-C. Nevertheless, for each sub-problem we imposed some fine-tuning parameters to make the problem tractable, which may impact the overall performance of problems (36) and (38) in a less controllable way. A closer look at two optimization problems reveals that the parameter τ_{th} in (36) reflects the MSE level, which is exactly the objective in (38), and similarly U_c^N in (38) specifies the minimum multiplexing gain, which is the objective of (36). As such, one may think to connect two optimization problems, so that the optimized objective function of one problem serves as the designing parameter in the other one. Therefore, we come up with Algorithm 1 to make the alternating projection between two sub-problems. In particular, Algorithm 1 takes the inputs of the bipartite graph representation constructed with a given threshold δ, and its adjacency matrix $\boldsymbol{A}$. Algorithm 1 starts with the initialization of user and beam selection parameters $\boldsymbol{x}$ and $\boldsymbol{y}$, which are all inactive at the beginning. The main procedure is the "while" loop that solves two sub-problems $\mathcal{P}_1''$ and $\mathcal{P}_2''$ in an iterative manner. In the iteration t, the sub-problem $\mathcal{P}_1''$ is first solved with an updated hyper-parameter τ_{th}^t. The solution of $\boldsymbol{x}^t$ and $\boldsymbol{y}^t$ is then updated and used to compute the number of active users U_c^N for $\mathcal{P}_2''$. Then the solution to $\mathcal{P}_2''$ updates $\boldsymbol{x}^t$ and $\boldsymbol{y}^t$, and the minimized objective updates MSE^t for the next iteration. The iteration terminates when it exceeds the maximum number $t_{\max}$, or the alternating projection converges such that the solution $\boldsymbol{x}^t$ does not change over iteration t. Thus, $\boldsymbol{x}^t$ and $\boldsymbol{y}^t$ at this point will be the final solution.

The complexity of Algorithm 1 involves both that of the alternating projection between two MILPs and that of solving MILPs. For the alternating projection, it only takes a few iterations before it converges. For solving the MILPs, the complexity depends on the implementations of the solvers, e.g., branch-and-bound. While MILPs are in general NP-hard problems, using the MATLAB function "intlinprog", it takes a few seconds on a desktop PC. It is challenging to theoretically analyze the complexity of the MILPs because of their combinatorial nature. Fortunately, Algorithm 1 is not required to compute frequently in practice. It is because $\mathcal{G}$ is constructed from the second-order statistics, i.e., the channel covariance matrices, which vary much slower than the instantaneous channels in low-to-moderate mobility scenarios. As such, we will instead evaluate the convergence performance of the algorithm by simulations in Section V.

V. Numerical Results

In this section, we detail the numerical results for the evaluation of the approaches proposed in Section IV in practical massive MIMO communication scenarios.

A. Simulation Scenario

We consider a single cell with $N_U=20$ randomly located single-antenna users. The channel via each scatter is composited of 20 paths, within AS of $\frac{\pi}{16}$. The base station is equipped with $M=128$ antennas, and these antennas are arranged with two different configurations: a rectangular 16×8 UPA and a 128×1 ULA. In all simulation results, we estimate the channel covariance matrix using 1000 uplink channel realizations. To capture the strong user-beam association, we construct a bipartite graph with a threshold parameter $\delta=4$.[1]

In this section, we evaluate the proposed on-off beam and user selection method using two performance metrics, i.e., the achievable sum rate and the normalized MSE (NMSE) per selected user in the cell. The achievable sum rate is averaged over the instantaneous sum rate of 1000 channel realizations, and the average NMSE per user is defined as

$$\text{NMSE}=\frac{1}{\sum_i y_i}\sum_{i=1}^{N_U}y_i\frac{\|\hat{\boldsymbol{h}}_i-\boldsymbol{h}_i\|^2}{\|\boldsymbol{h}_i\|^2} \tag{39}$$

where the average is over the active users. Note that the sum rate performance is determined by both channel estimation accuracy (i.e., NMSE per user) and the number of activated users. Unless otherwise explicitly specified, for each separate optimization problem, we choose the following parameters: the MSE threshold $\tau_{\text{th}}=0.2$, SINR threshold $\tau=0.7$, $p=3$, and the minimum number of users to be selected $U_c^N=5$.

For channel estimation and beamformer design, we take into account the insights obtained from asymptotic analysis, in addition to those for finite antenna cases. Table I summarizes

[1]This hyper-parameter δ determines the density of the bipartite graph representation. A larger δ gives us a sparser bipartite graph for the MILP problems – it offers more freedom for beam/user selection, while the residual interference (i.e., those edges with weight smaller than δ are not considered in MILPs) is not under control. In contrast, a smaller δ gives us a denser bipartite graph, which takes into account more edges in the graph, but it may result in restrictive solutions to MILPs and therefore non-ideal beam/user selection. In general, it is a challenging task to find the optimal value of the threshold δ that achieves the best performance in a principled way. Instead, we choose the threshold δ based on the proportion of the sum edge-weights in the bipartite graph. In the simulation, choosing $\delta=4$, the bipartite graph representation captures 80% total weights of all edges.

TABLE I: Uplink channel estimation and receive beamformer design

	Channel Estimation	Beamforming
MMSE	$\hat{\boldsymbol{h}}_i^{\text{MMSE}}$	$\boldsymbol{w}_i$
k-means$_0$	$\hat{\boldsymbol{h}}_i^{\text{k-means}}$	$\boldsymbol{w}_i^{\text{k-means}}$
k-means$_\infty$	$\hat{\boldsymbol{h}}_i^{\text{k-means}}$	$\boldsymbol{w}_i^{\text{k-means}}$
ON-OFF$_{0,0}$	$\hat{\boldsymbol{h}}_i^{\text{ON/OFF}}$	$\boldsymbol{w}_i^{\text{ON/OFF}}$
ON-OFF$_{0,\infty}$	$\hat{\boldsymbol{h}}_i^{\text{ON/OFF}}$	$\boldsymbol{w}_{i,\infty}^{\text{ON/OFF}}$
ON-OFF$_{\infty,0}$	$\hat{\boldsymbol{h}}_{i,\infty}^{\text{ON/OFF}}$	$\boldsymbol{w}_i^{\text{ON/OFF}}$
ON-OFF$_{\infty,\infty}$	$\hat{\boldsymbol{h}}_{i,\infty}^{\text{ON/OFF}}$	$\boldsymbol{w}_{i,\infty}^{\text{ON/OFF}}$

various schemes using different channel estimation and beamforming design. In this table, the ON-OFF methods are based on our proposed joint user and beam selection. To evaluate how asymptotic results apply to the practical settings with a finite number of antennas, we also include the asymptotic channel estimate $\hat{\boldsymbol{h}}_{i,\infty}^{\text{ON/OFF}}$ and precoding vector $\boldsymbol{w}_{i,\infty}^{\text{ON/OFF}}$ for comparison. The subscripts with ∞ of ON-OFF indicate an asymptotic estimator or beamformer is employed. For the sake of comparison, we also consider the MMSE algorithm with all users and beams are selected as well as a user selection scheme with k-means clustering.

For channel estimation, $\hat{\boldsymbol{h}}_i^{\text{MMSE}}$, $\hat{\boldsymbol{h}}_i^{\text{ON/OFF}}$, and $\hat{\boldsymbol{h}}_{i,\infty}^{\text{ON/OFF}}$ are defined in (11), (23), and (24) respectively, whereas $\hat{\boldsymbol{h}}_i^{\text{k-means}}$ is defined similarly to (11) with the only difference that only the selected users from different k-means clusters are taken into account instead of the all N_U users. Similarly, for beamforming design, $\boldsymbol{w}_i^{\text{ON/OFF}}$ and $\boldsymbol{w}_{i,\infty}^{\text{ON/OFF}}$ are defined in (28) and (29), respectively. For the beamformers used for MMSE schemes, $\boldsymbol{w}_i$ can be obtained from $\boldsymbol{w}_i^{\text{ON/OFF}}$ by letting all users be active. Similarly, $\boldsymbol{w}_i^{\text{k-means}}$ can be obtained by activating users selected from k-means clustering.

Both k-means$_0$ and k-means$_\infty$ follow the standard k-means clustering algorithm, where the goal is to divide data points into clusters so that the similar data points are grouped in a cluster with a common centroid. The objective function is the minimization of the sum of Euclidean distance between each data point and its associated centroid. In our setting, users are firstly clustered using k-means according to their covariance matrices, and only one user is selected from one cluster for simultaneous transmission. The difference between k-means$_0$ and k-means$_\infty$ lies in the distinct data considered for clustering, and therefore distinct similarity measure and centroid generation strategies [4], [30]. In particular, for k-means$_0$, the dominant eigenspaces and its chordal distance are applied as data points and similarity measure, respectively, as did in joint spatial division and multiplexing (JSDM) for user grouping in FDD massive MIMO [6]. In contrast to the k-means$_0$ scheme, k-means$_\infty$ takes advantage of channels' asymptotic representation as suggested in Theorem 1. In particular, as the user i's covariance matrix $\boldsymbol{R}_i$ can be diagonalized by 2D-DFT matrix into a diagonal matrix $\boldsymbol{\Lambda}_i$, we use the reshaped vector from $\text{diag}(\boldsymbol{\Lambda}_i)$ as the data point for the k-means clustering.

For the k-means clustering based user selection algorithms, i.e., k-means$_0$ and k-means$_\infty$, the number of clusters is required to be known *a prior*. Instead of finding the number of clusters directly using e.g., [30], the number of active users from optimizing (36) is served as the number of clusters. The performance of clustering algorithms highly relies on initialization. To rectify this, we run several times of experiments with different initializations and finally choose the best performance of k-means for comparison.

TABLE II: The settings of simulations

Objectives	Metrics	Antenna Configurations	
		16×8	128×1
(36)	Sum Rate	Fig. 3	Fig. 4
(36)	NMSE	Fig. 5	Fig. 6
(38)	Sum Rate	Fig. 7	Fig. 8
(38)	NMSE	Fig. 9	Fig. 10

B. Simulation Results and Analysis

We first consider two objectives of sum rate maximization as in Theorem 3, and MSE minimization as in Theorem 4 separately, followed by the joint optimization via alternating projection as in Algorithm 1. Table II summarizes the settings of the following figures corresponding to different objectives and performance metrics.

1) Sum Rate Maximization: In Figures 3-6, we show the sum rate and the NMSE performance versus SNR for the uplink data transmission and channel estimation, respectively, with respect to 16×8 UPA and 128×1 ULA antenna configurations. For our proposed ON-OFF schemes, the joint beam and user selection results from (36) in Theorem 3, in which the objective is the sum rate maximization. Note that the estimated channels of ON-OFF$_{0,0}$ and ON-OFF$_{\infty,\infty}$ are $\hat{\boldsymbol{h}}_i^{\text{ON/OFF}}$ and $\hat{\boldsymbol{h}}_{i,\infty}^{\text{ON/OFF}}$, which are identical to that of ON-OFF$_{0,\infty}$ and ON-OFF$_{\infty,0}$, respectively, so we only keep one of them in figures.

It is shown in Fig. 3 and Fig. 4 that our proposed ON-OFF method ON-OFF$_{0,0}$ outperforms MMSE and k-means clustering algorithms in both sum rate and NMSE performance, thanks to the effective joint beam and user selection. In Fig. 3, the MMSE and the asymptotic versions of ON-OFF schemes, i.e., ON-OFF$_{0,\infty}$, ON-OFF$_{\infty,0}$ and ON-OFF$_{\infty,\infty}$, suffer from sum rate saturation in the high SNR regime. For the MMSE scheme, because all users are active, the multiuser interference is severe due to high channel correlation among users, so that both sum rate and NMSE performance do not decrease as SNR increases. This confirms that user selection is crucial for a massive MIMO system with a large number (e.g., 20) of users. The sum rate saturation of those ON-OFF methods is due to the fact that the asymptotic treatment of channel estimation and precoding with finite antennas leaves too much interference so that the system is interference-limited. The sum rate performance of ON-OFF$_{0,\infty}$ and ON-OFF$_{\infty,\infty}$ is worse than those of ON-OFF$_{0,0}$ and ON-OFF$_{\infty,0}$, which reveals that the asymptotic treatment with interference ignored deteriorates more on precoding than channel estimation. This demonstrates that the asymptotic results should be refined to adapt the practical scenarios.

For clustering algorithms, both sum rate and NMSE performance of k-means$_0$ is better than that of k-means$_\infty$, due to the inaccuracy of asymptotic representation under the finite number of both column and row antennas. It appears the sum rate of k-means is even worse than that of MMSE in the low

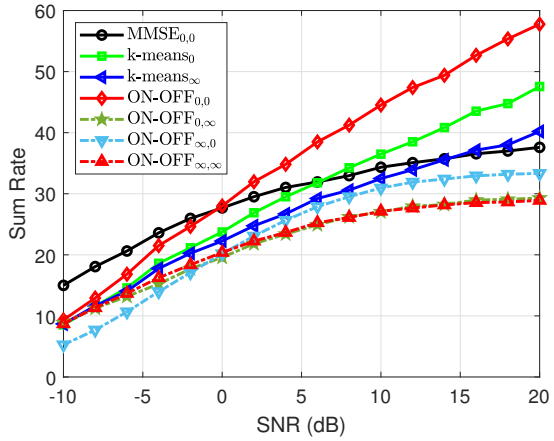

Fig. 3: Sum rate versus SNR with 16×8 UPA. The on-off parameters are obtained from (36), and there are 5 clusters for k-means.

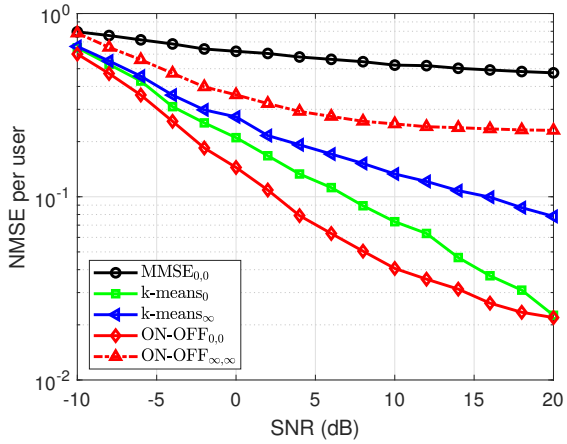

Fig. 4: NMSE versus SNR for 16×8 UPA. The on-off parameters are obtained from (36), and there are 5 clusters for k-means.

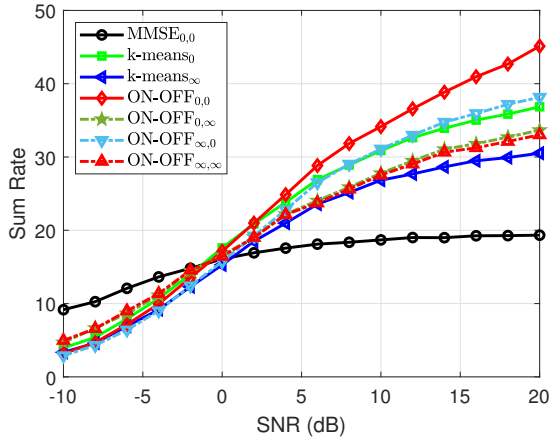

Fig. 5: Sum rate versus SNR with 128 ULA. The on-off parameters are from (36), and 5 clusters for k-means.

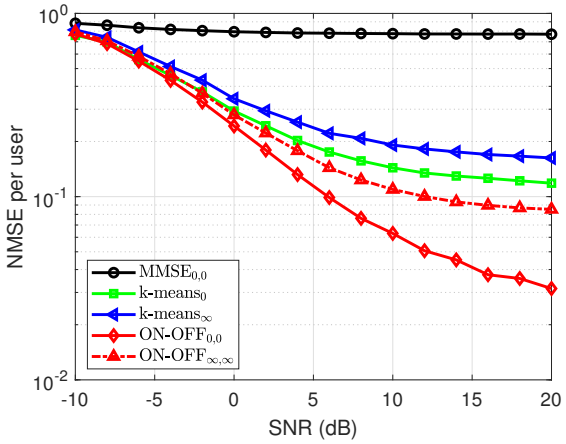

Fig. 6: NMSE versus SNR with 128 ULA. The on-off parameters are from (36), and 5 clusters for k-means.

and moderate SNR regimes - it is probably because the high channel correlation makes the number of users that can be selected quite limited. In contrast, our proposed method has better performance than that of MMSE with the same number of activated users. There are two limitations of the k-means-type algorithms. On one hand, k-means algorithms rely critically on the initialization of centroids - a worse initialization leads to inferior results. On the other hand, k-means algorithms minimize the distance of the data points within the cluster, ignoring the distance between clusters, which may result in overlapping user selection if clusters are not clearly separable.

Fig. 5 and Fig. 6 present the similar results as Fig. 3 and Fig. 4, but a 128×1 ULA antenna configuration is considered. The observations are similar to those of Fig. 3 and Fig. 4, which confirms that our proposed methods are valid for both the UPA and ULA settings. In contrast, the asymptotic versions of the ON-OFF scheme gain certain improvement. In particular, compared with Fig. 4, the ON-OFF scheme with asymptotic channel estimation, i.e., ON-OFF$_{\infty,0}$, has improved sum rate performance, which outperforms that of MMSE and k-means-like algorithms. The reason is that, as squeezing the UPA to a ULA with the same number of antennas, the asymptotic channel representation becomes more accurate, so that asymptotic channel estimation still works in a non-asymptotic setting.

2) MSE Minimization: Figures 7-10 illustrate the sum rate and NMSE performance versus SNR in the same setting as those in Figures 3-6. The difference is that the joint beam and user selection comes from the optimization problem (38), where the main target is MSE minimization. Remarkably, with proper chosen threshold parameters, the sum rate and NMSE performance using the joint beam and user selection from (38) is comparable with that using (36) both for UPA and ULA antenna configurations. It is worth noting that, when serving the same number of users, UPA (Figures 3 and 7) has a better sum rate performance than ULA (Figures 5 and 9). It is possibly because there are too many activated users in ULA (Figures 5 and 9) that lead to certain overlapping among users. It demonstrates that the UPA antenna could be able to serve more users than ULA, which also is one of the advantages of the UPA system.

In order to avoid relying too much on threshold parameters, we proposed to use an alternating projection algorithm in Section IV-D to solve the sum rate maximization problem (36) and the MSE minimization problem (38) in an iterative manner.

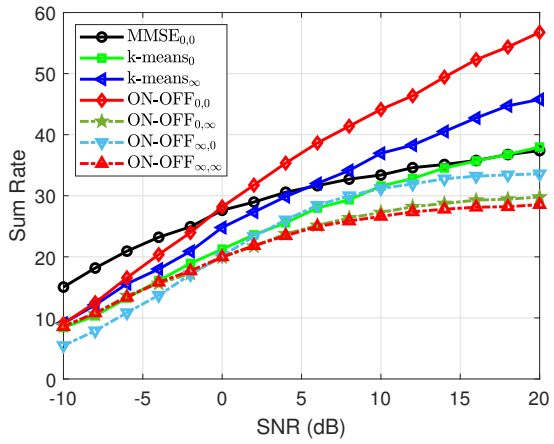

Fig. 7: Sum rate versus SNR with 16×8 UPA. The on-off parameters are obtained from (38), and there are 5 clusters for k-means.

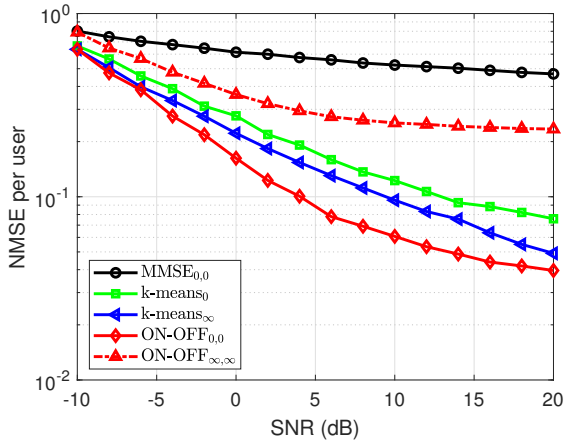

Fig. 8: NMSE versus SNR with 16×8 UPA. The on-off parameters are obtained from (38), and there are 5 clusters for k-means.

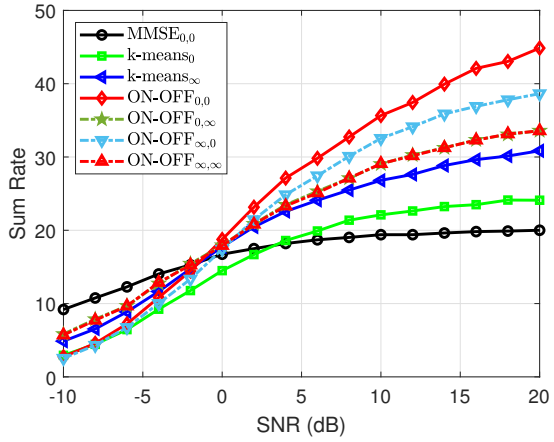

Fig. 9: Sum Rate versus SNR with 128 ULA. The on-off parameters are from (38), and 5 clusters for k-means.

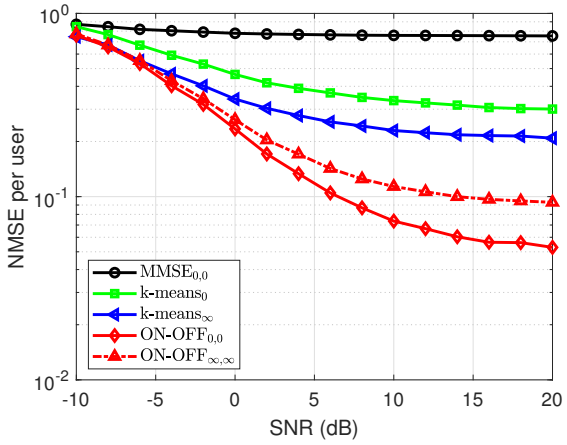

Fig. 10: NMSE versus SNR with 128 ULA. The on-off parameters are from (38), and 5 clusters for k-means.

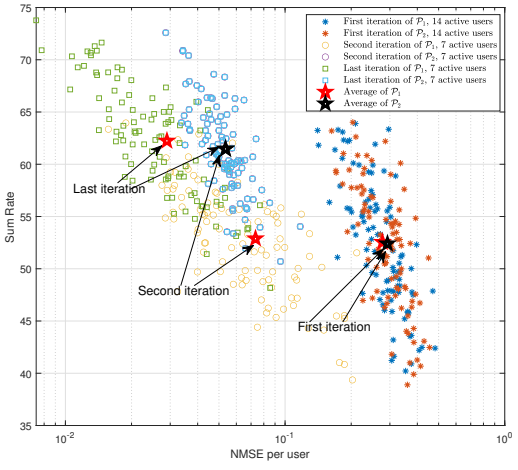

Fig. 11: Instantaneous sum rate versus NMSE at 20 dB with 16×8 UPA. The on-off parameters are from Alg. 1.

3) Alternating Projection: Fig. 11 presents the instantaneous sum rate versus NMSE performance obtained from Algorithm 1 with SNR $= 20$ dB and 16×8 UPA antennas. Each point is a pair of instantaneous sum rate and NMSE for a channel realization. The joint beam and user selection comes from the solutions to (36) and (38). We adopt the SINR threshold $\tau = 0.7$ to ensure a feasible solution that could be found by both (36) and (38). The instantaneous sum rate and MSE are calculated by using our proposed scheme ON-OFF$_{0,0}$. The alternating projection algorithm is able to converge within a few iterations (3 iterations in Fig. 11). The MSE threshold τ_{th} is 0.95 as the initialization, which means the MSE constraint (36g) is relaxed, so that the optimization is prone to sum rate maximization. As observed from Fig. 11, almost all the (rate, NMSE) pairs from the last iteration of alternating projection concentrate on a small area, which yields a reasonably good average sum rate and NMSE (marked as stars). It shows that the average sum rate performance obtained from alternating projection in Fig. 11 is much better than that of the separate rate or MSE optimization as in Fig. 3, Fig. 4, Fig. 7 and Fig. 8 obtained from (36) or (38). This demonstrates that the alternating projection algorithm is capable to adjust the parameters τ_{th} and U_c^N automatically so as to lead optimization towards higher sum rate performance. With respect to the

selected users, the first iteration has 14 users selected, but this number is decreased to 7 in the last iteration after the alternating projection algorithm. This is also in contrast to the number of selected users in Fig. 3, Fig. 4, Fig. 7 and Fig. 8, where only 5 users are selected. In addition, such an alternating algorithm does not require to initialize the number of activated users, which is one of the critical initial conditions for k-means algorithms.

VI. Conclusion

In this paper, we considered the joint uplink channel estimation and data transmission in the overloaded multiuser uplink massive MIMO network with UPA antennas at the base station. To mitigate channel spatial correlation due to the collocation of antenna elements and users, we adopted the recently proposed ACS concept and developed an effective joint beam and user selection method to artificially sparsify the effective users' channels. In particular, we first leveraged the doubly block Toeplitz structure of channel covariance matrices when UPA is deployed, and approximately represented users' channels by common basis vectors coming from the 2D-DFT matrix. By such approximate representation, we proposed a joint beam and user selection method via ACS to reduce the spatial correlation among the selected users. By a weighted bipartite graph representation of user-beam association, we translated the joint beam and user selection problem into mixed integer linear programs (MILPs), which can be solved in a more tractable way. The alternating projection between two MILPs yields better performance than each of them with automatic hyper-parameter fine-tuning. This is another evidence showing the powerfulness of the ACS concept in massive MIMO systems beyond the use for downlink channel reconstruction in FDD mode. It is expected this concept has more application scenarios to deal with spatial correlation in both TDD and FDD massive MIMO systems.

Appendix

A. Proof of Theorem 1

We first show that $\boldsymbol{R}$ is a doubly block Toeplitz matrix. For notational convenience, we define

$$\Omega = \{(\theta, \phi) : \theta \in \mathcal{A}, \phi \in \mathcal{B}\}. \tag{40}$$

Given the channel vector $\boldsymbol{h}$ in (1), the covariance matrix $\boldsymbol{R} = \mathbb{E}\{\boldsymbol{h}\boldsymbol{h}^{\mathsf{H}}\}$ can be written as

$$\boldsymbol{R} = \mathbb{E}\int_{\Omega}\int_{\Omega'} \beta(\theta,\phi)\beta^*(\theta',\phi')\boldsymbol{a}(\theta,\phi)\boldsymbol{a}^{\mathsf{H}}(\theta',\phi')d\theta d\phi d\theta' d\phi' \tag{41}$$

$$= \beta\int_{\Omega} \boldsymbol{a}(\theta,\phi)\boldsymbol{a}^{\mathsf{H}}(\theta,\phi)d\theta d\phi \tag{42}$$

due to the fact that $\beta(\theta,\phi)$ is i.i.d. across paths, i.e.,

$$\mathbb{E}\{\beta(\theta,\phi)\beta^*(\theta',\phi')\} = \begin{cases} \beta, & (\theta,\phi) = (\theta',\phi') \\ 0, & \text{otherwise} \end{cases}. \tag{43}$$

Plugging (2) into (42), we have

$$\boldsymbol{R} = \beta\int_{\Omega} \boldsymbol{a}_y(\theta,\phi)\boldsymbol{a}_y^{\mathsf{H}}(\theta,\phi) \otimes \boldsymbol{a}_x(\theta,\phi)\boldsymbol{a}_x^{\mathsf{H}}(\theta,\phi)d\theta d\phi \tag{44}$$

$$= \beta\int_{\Omega} \begin{bmatrix} \boldsymbol{B}_{11} & \cdots & \boldsymbol{B}_{1M_y} \\ \vdots & \ddots & \vdots \\ \boldsymbol{B}_{M_y1} & \cdots & \boldsymbol{B}_{M_yM_y} \end{bmatrix} d\theta d\phi \tag{45}$$

where each block $\boldsymbol{B}_{pq}$ can be written as

$$\boldsymbol{B}_{pq} = \left[\boldsymbol{a}_y(\theta,\phi)\boldsymbol{a}_y^{\mathsf{H}}(\theta,\phi)\right]_{pq}\boldsymbol{A}(\theta,\phi) \tag{46}$$

$$= e^{\jmath\frac{2\pi}{\lambda_w}d_y(p-q)\sin\phi\sin\theta}\boldsymbol{A}(\theta,\phi) \tag{47}$$

with

$$[\boldsymbol{A}(\theta,\phi)]_{ij} = [\boldsymbol{a}_x(\theta,\phi)]_i[\boldsymbol{a}_x^{\mathsf{H}}(\theta,\phi)]_j = e^{\jmath\frac{2\pi}{\lambda_w}d_x(i-j)\sin\phi\cos\theta}. \tag{48}$$

It can be easily verified that $[\boldsymbol{A}(\theta,\phi)]_{ij}$ only depends on $i-j$, by which it is deemed as a Toeplitz matrix. Moreover, $\boldsymbol{A}(\theta,\phi)$ is a Hermitian matrix as $\boldsymbol{A}(\theta,\phi) = \boldsymbol{A}^{\mathsf{H}}(\theta,\phi)$. Similarly, $\boldsymbol{B}_{pq}$ only depends on $p-q$ and thus $\boldsymbol{R}$ is a block Toeplitz matrix with Toeplitz blocks, which is referred to as a doubly block Toeplitz matrix. Further, $\boldsymbol{R}$ is a Hermitian matrix, as $\boldsymbol{R} = \boldsymbol{R}^{\mathsf{H}}$.

In (45), as the integral is element-wise operation, which does not change the Toeplitz structure of the matrix, we conclude that $\boldsymbol{R}$ is still a Hermitian doubly block Toeplitz matrix. That is, $\boldsymbol{R}$ has $M_y \times M_y$ blocks with Toeplitz structure and each $M_x \times M_x$ block is a Toeplitz matrix.

According to [31] and [32], the Hermitian doubly block Toeplitz matrix $\boldsymbol{R}$ is asymptotically equivalent to the corresponding doubly block circulant matrix $\boldsymbol{C}$, which can be decomposed by 2D-DFT matrix, i.e.,

$$\boldsymbol{C} = (\boldsymbol{V}_{M_y} \otimes \boldsymbol{V}_{M_x})\boldsymbol{\Lambda}(\boldsymbol{V}_{M_y} \otimes \boldsymbol{V}_{M_x})^{\mathsf{H}} \tag{49}$$

$$= \sum_{a=1}^{M_y}\sum_{b=1}^{M_x} \chi(\omega_a,\zeta_b)(\boldsymbol{f}_a \otimes \boldsymbol{g}_b)(\boldsymbol{f}_a \otimes \boldsymbol{g}_b)^{\mathsf{H}} \tag{50}$$

where $\boldsymbol{f}_a$ and $\boldsymbol{g}_b$ are the a-th and b-th columns of DFT matrices $\boldsymbol{V}_{M_y}$ and $\boldsymbol{V}_{M_x}$, respectively. The scalar-valued function $\chi(\omega,\zeta)$ is referred to the generating function of the doubly block Toeplitz matrix $\boldsymbol{R}$ and the doubly block circulant matrix $\boldsymbol{C}$, i.e.,

$$\chi(\omega,\zeta) = \sum_{\mu}\sum_{\nu} r_{\mu,\nu}e^{\jmath 2\pi(\mu\omega+\nu\zeta)} \tag{51}$$

with $\mu \in [-M_y, M_y], \nu \in [-M_x, M_x]$, where

$$r_{\mu,\nu} = \beta\int_{\mathcal{B}}\int_{\mathcal{A}} e^{-\jmath\frac{2\pi}{\lambda_w}(d_x\nu+d_y\mu)\sin\phi\sin\theta}d\theta d\phi \tag{52}$$

is the ν-th element of μ-th block matrix of $\boldsymbol{R}$. For $(\omega_a,\zeta_b) = (\frac{a-1}{2M_y}, \frac{b-1}{2M_x})$, $\chi(\omega_a,\zeta_b)$ is the uniform sampling of the continuous and periodic function $\chi(\omega,\zeta)$, and it can be seen as the eigenvalues of $\boldsymbol{R}$ when $M_x, M_y \to \infty$. Nevertheless, in practical UPA system with a finite number of antennas, $\boldsymbol{R}$ is not perfectly diagonalizable by 2D-DFT matrices. That is, $\boldsymbol{\Lambda}$ is not a diagonal matrix any more. As such, $\chi(\omega_a,\zeta_b)$ is used as an approximation of the eigenvalues of $\boldsymbol{R}$.

B. Proof of Theorem 3

For the objective function, we follow the footsteps in [20] and introduce a set of binary variables $z_{i,m} \in [0,1]$.

$$\max_{x_m, y_i, z_{i,m}} \sum_{b_m \in \mathcal{B}}\sum_{u_i \in \mathcal{U}} z_{i,m} \tag{53a}$$

$$\text{s.t.} \quad x_m \le \sum_{u_i \in \mathcal{U}} [\boldsymbol{A}]_{i,m} y_i, \quad \forall b_m \in \mathcal{B}, \tag{53b}$$

$$y_i \le \sum_{b_m \in \mathcal{B}} [\boldsymbol{A}]_{i,m} x_m, \quad \forall u_i \in \mathcal{U}, \tag{53c}$$

$$z_{i,m} \le [\boldsymbol{A}]_{i,m}, \quad \forall u_i \in \mathcal{U},\ b_m \in \mathcal{B}, \tag{53d}$$

$$\sum_{u_i \in \mathcal{U}} z_{i,m} \le x_m, \quad \forall b_m \in \mathcal{B}, \tag{53e}$$

$$\sum_{b_m \in \mathcal{B}} z_{i,m} \le y_i, \quad \forall u_i \in \mathcal{U}, \tag{53f}$$

$$x_m, y_i \in \{0,1\}, \quad \forall u_i \in \mathcal{U},\ b_m \in \mathcal{B}, \tag{53g}$$

$$z_{i,m} \in [0,1], \quad \forall u_i \in \mathcal{U},\ b_m \in \mathcal{B}, \tag{53h}$$

where (53b)-(53c) ensure that, if a beam is selected, there should be a user to occupy it, and vice versa, the objective function (53a) and the constraints (53d)-(53f) are obtained by following the similar footsteps in [20] for which the edges $\{(u_i, b_m) : z_{i,m} = 1\}$ in the selected subgraph $\mathcal{G}' = (\mathcal{B}', \mathcal{U}', \mathcal{E}')$ form a maximum cardinality matching.

To simplify the constraints in a form of inequalities, we consider the original graph $\mathcal{G} = (\mathcal{U}, \mathcal{B}, \mathcal{E})$ in lieu of the selected subgraph $\mathcal{G} = (\mathcal{U}', \mathcal{B}', \mathcal{E}')$ where $x_m = 1$ and $y_i = 1$ if and only if $u_i \in \mathcal{U}'$ and $b_m \in \mathcal{B}'$. Thus, from (35b), we have

$$y_i \sum_{m=1}^{M} \lambda_{i,m} \left(1 - \frac{\lambda_{i,m} x_m}{\sum_{j=1}^{N_U} y_j \lambda_{j,m} x_m + \sigma^2}\right) \le P_i, \quad \forall u_i \in \mathcal{U}. \tag{54}$$

Accordingly, if beam m has a significant contribution to the channel representation in the beam domain, it is better to be selected so the corresponding MSE can be mitigated; otherwise, the beam can not selected (i.e., $x_m = 0$). As such, instead of considering all beams for each user jointly, we investigate each beams separately. To this end, we introduce an auxiliary variable $\tau_{\text{th}} \in [0,1]$ such that $\tau_{\text{th}} \sum_{m=1}^{M} \lambda_{i,m} = P_i$.

To make (54) more tractable, we place our focus on the regime with high SNR, where $\sigma^2 \to 0$, in hope to gain insights that can guide the design in the practical settings. As such, constraint (54) can be replaced by a simpler yet more restrictive constraint as

$$y_i \left(1 - \frac{\lambda_{i,m} x_m}{\sum_{j=1}^{N_U} y_j \lambda_{j,m}}\right) \le \tau_{\text{th}}, \quad \forall u_i \in \mathcal{U}, \forall b_m \in \mathcal{B}, \tag{55}$$

where x_m in the denominator is dropped without loss of feasibility as it does not change the inequality given $x_m \in \{0,1\}$. This constraint is more restrictive in the sense that if this one is satisfied, then (35b) is satisfied automatically. This guarantees a feasible solution to (35).

By this constraint, the beams that contribute much to user-i's effective channel representation in the beam domain (i.e., with a large $\lambda_{i,m}$) are more likely selected, and this constraint ensures that the MSE of estimating the component of user-i's channel projected onto beam-m is mitigated. The beams with little contribution (i.e., with a small $\lambda_{i,m}$) can be or not be selected. Nevertheless, in case a beam should be unselected for some reason, it may also result in the non-selection of the users who relies very much on that.

A further manipulation transforms constraint (55) into the following form:

$$y_i \sum_{j=1}^{N_U} y_j \lambda_{j,m} - x_m y_i \lambda_{i,m} \le \tau_{\text{th}} \sum_{j=1}^{N_U} y_j \lambda_{j,m} \tag{56}$$

which can be transformed further to

$$(1 - \tau_{\text{th}}) \sum_{j=1}^{N_U} y_j \lambda_{j,m} \le x_m \lambda_{i,m} + c_1(1 - x_m) + c_2(1 - y_i) \tag{57}$$

where the constants c_1 and c_2 are sufficiently large to make sure that if user i or beam m is not selected (i.e., $y_i = 0$ or $x_m = 0$) then this constraint is automatically satisfied.

As a matter of fact, (55) can be also rewritten as follows

$$y_i \sum_{j \ne i}^{N_U} y_j \lambda_{j,m} x_m \le \tau_{\text{th}} \sum_{j=1}^{N_U} y_j \lambda_{j,m} x_m \tag{58}$$

because $y_i = y_i^2$ given that $y_i \in \{0,1\}$. Intuitively, if both user i and beam m are selected, the other users can be also selected if the overall interference from $j \ne i$ to beam m accounts for a fraction (τ_{th}) of the overall power seen at beam m including the power of the desired signal from user i. Further, with respect to the SINR constraint (35c), it can be specified as

$$\frac{\sum_m \lambda_{i,m} x_m}{\sum_{j \ne i} \sum_m y_j \lambda_{j,m} x_m + \sigma^2} \ge y_i \Gamma_i, \quad \forall u_i \in \mathcal{U}. \tag{59}$$

Plugging (58) into (59), we can transform (59) into a more restrictive one as follows

$$\sum_{m=1}^{M} \lambda_{i,m} x_m \ge y_i \Gamma_i \sigma^2 + y_i \Gamma_i \tau_{\text{th}} \sum_{m=1}^{M} \sum_{j=1}^{N_U} y_j \lambda_{j,m} x_m \tag{60}$$

where the two terms on the RHS correspond to desired signal and upper bounded interference power, respectively. We further split the above inequality into the following two constraints

$$\sum_{m=1}^{M} \lambda_{i,m} x_m \ge y_i \Gamma_i \ (\sigma^2 + \kappa) \tag{61}$$

$$\kappa \ge y_i \tau_{\text{th}} \sum_{m=1}^{M} \sum_{j=1}^{N_U} y_j \lambda_{j,m} x_m \tag{62}$$

where Γ_i and κ are SINR and INR thresholds, respectively.

By letting $\kappa = \tau_{\text{th}} \sum_m \tau_\omega^m$, we can replace (62) by a simpler yet more restrictive constraint to ensure this condition, that is,

$$\sum_{i=1}^{N_U} y_i \lambda_{i,m} \le x_m \tau_\omega^m \quad \forall b_m \in \mathcal{B} \tag{63}$$

where $\tau_\omega^m = \max_p \{\lambda_{i,m}, i \in [N_U]\}$.

To make it more tractable, we introduce a designing parameter $\tau \in [0,1]$ such that $\Gamma_i + \kappa = \frac{\tau \sum_m \lambda_{i,m}}{\sigma^2}$. Thus, we have

$$y_i \tau \sum_{m=1}^{M} \lambda_{i,m} \le \sum_{m=1}^{M} \lambda_{i,m} x_m \quad \forall u_i \in \mathcal{U}. \tag{64}$$

Collecting all inequalities above gives us the MILP formulation in Theorem 3.

C. Proof of Theorem 4

The optimization problem $(\mathcal{P}_2')$ can be translated into a more concrete form as follows:

$$\min_{x_m, y_i} \sum_{i=1}^{N_U} \sum_{m=1}^{M} y_i \lambda_{i,m} \left(1 - \frac{\lambda_{i,m} x_m}{\sum_{j=1}^{N_U} y_j \lambda_{j,m}}\right) \tag{65a}$$

$$\text{s.t.} \quad (36h), (36i) \tag{65b}$$

$$\sum_{i=1}^{N_U} y_i \geq U_c^N, \tag{65c}$$

$$x_m, y_i \in \{0,1\}, \quad \forall b_m \in \mathcal{B},\ u_i \in \mathcal{U} \tag{65d}$$

where we directly impose a constraint that the number of active users is no less than a predefined parameter U_c^N for simplicity, because the multiplexing gain is mainly determined by the number of users given $N_U \ll M$.

To simplify the quantities in the objective function, we introduce a set of auxiliary variables $\{t_{i,m}\}$, so that (65a) can be rewritten as

$$\min_{x_m, y_i, t_{i,m}} \sum_{i=1}^{N_U} \sum_{m=1}^{M} (y_i \lambda_{i,m} + t_{i,m}) \tag{66a}$$

$$\text{s.t.} \quad -\frac{x_m \sum_{i=1}^{N_U} y_i \lambda_{i,m}^2}{\sum_{j=1}^{N_U} y_j \lambda_{j,m}} \leq \sum_{i=1}^{N_U} t_{i,m}, \quad \forall b_m \in \mathcal{B}' \tag{66b}$$

$$t_{i,m} \leq 0, \quad \forall b_m \in \mathcal{B},\ u_i \in \mathcal{U}. \tag{66c}$$

Given the fact that

$$\frac{\sum_{i=1}^{N_U} y_i \lambda_{i,m}^2}{\sum_{j=1}^{N_U} y_j \lambda_{j,m}} = \frac{(\sum_{i=1}^{N_U} y_i \lambda_{i,m})^2 - \sum_{i,j:i\neq j} y_i y_j \lambda_{i,m} \lambda_{j,m}}{\sum_{j=1}^{N_U} y_j \lambda_{j,m}} \tag{67}$$

$$\geq \sum_{i=1}^{N_U} y_i \lambda_{i,m} - \sum_{i,j:i\neq j} y_i y_j \lambda_{i,m} \lambda_{j,m} \tag{68}$$

where the inequality is because of $\sum_{j=1}^{N_U} y_j \lambda_{j,m} \geq 1$ almost surely, the constraint (66b) can be replaced by a more restrictive yet tractable one as below

$$-x_m \sum_{i=1}^{N_U} \left(y_i \lambda_{i,m} - \sum_{j:j\neq i} y_i y_j \lambda_{i,m} \lambda_{j,m} \right) \leq \sum_{i=1}^{N_U} t_{i,m}. \tag{69}$$

By considering each user i separately, we further restrict this constraint with a more tractable one

$$-\lambda_{i,m} + \sum_{j:j\neq i} y_j \lambda_{i,m} \lambda_{j,m} - t_{i,m} \leq c_3(1 - x_m) + c_4(1 - y_i), \quad \forall u_i \in \mathcal{U},\ b_m \in \mathcal{B} \tag{70}$$

where $c_3, c_4 > 0$ are sufficiently large constants to guarantee that the constraint is automatically satisfied if the beam m or the user i is not selected. Collecting all inequalities above gives us the MILP formulation in Theorem 4.

REFERENCES

[1] T. L. Marzetta, "Noncooperative cellular wireless with unlimited numbers of base station antennas," *IEEE Transactions on Wireless Communications*, vol. 9, no. 11, pp. 3590–3600, 2010.

[2] E. G. Larsson, O. Edfors, F. Tufvesson, and T. L. Marzetta, "Massive MIMO for next generation wireless systems," *IEEE Communications Magazine*, vol. 52, no. 2, pp. 186–195, 2014.

[3] H. Yin, D. Gesbert, M. Filippou, and Y. Liu, "A coordinated approach to channel estimation in large-scale multiple-antenna systems," *IEEE Journal on Selected Areas in Communications*, vol. 31, no. 2, pp. 264–273, 2013.

[4] A. Adhikary, J. Nam, J. Ahn, and G. Caire, "Joint spatial division and multiplexing—the large-scale array regime," *IEEE Transactions on Information Theory*, vol. 59, no. 10, pp. 6441–6463, 2013.

[5] L. You, X. Gao, X.-G. Xia, N. Ma, and Y. Peng, "Pilot reuse for massive MIMO transmission over spatially correlated Rayleigh fading channels," *IEEE Transactions on Wireless Communications*, vol. 14, no. 6, pp. 3352–3366, 2015.

[6] J. Nam, A. Adhikary, J. Ahn, and G. Caire, "Joint spatial division and multiplexing: Opportunistic beamforming, user grouping and simplified downlink scheduling," *IEEE Journal of Selected Topics in Signal Processing*, vol. 8, no. 5, pp. 876–890, 2014.

[7] C.-K. Wen, S. Jin, K.-K. Wong, J.-C. Chen, and P. Ting, "Channel estimation for massive MIMO using Gaussian-mixture Bayesian learning," *IEEE Transactions on Wireless Communications*, vol. 14, no. 3, pp. 1356–1368, 2014.

[8] Z. Chen and C. Yang, "Pilot decontamination in wideband massive MIMO systems by exploiting channel sparsity," *IEEE Transactions on Wireless Communications*, vol. 15, no. 7, pp. 5087–5100, 2016.

[9] H. Yin, L. Cottatellucci, D. Gesbert, R. R. Müller, and G. He, "Robust pilot decontamination based on joint angle and power domain discrimination," *IEEE Transactions on Signal Processing*, vol. 64, no. 11, pp. 2990–3003, 2016.

[10] S. Haghighatshoar and G. Caire, "Massive MIMO pilot decontamination and channel interpolation via wideband sparse channel estimation," *IEEE Transactions on Wireless Communications*, vol. 16, no. 12, pp. 8316–8332, 2017.

[11] L. You, X. Gao, A. L. Swindlehurst, and W. Zhong, "Channel acquisition for massive MIMO-OFDM with adjustable phase shift pilots," *IEEE Transactions on Signal Processing*, vol. 64, no. 6, pp. 1461–1476, 2015.

[12] X. Rao and V. K. N. Lau, "Distributed compressive CSIT estimation and feedback for FDD multi-user massive MIMO systems," *IEEE Transactions on Signal Processing*, vol. 62, no. 12, pp. 3261–3271, 2014.

[13] Z. Gao, L. Dai, Z. Wang, and S. Chen, "Spatially common sparsity based adaptive channel estimation and feedback for FDD massive MIMO," *IEEE Transactions on Signal Processing*, vol. 63, no. 23, pp. 6169–6183, 2015.

[14] S. Haghighatshoar and G. Caire, "Massive MIMO channel subspace estimation from low-dimensional projections," *IEEE Transactions on Signal Processing*, vol. 65, no. 2, pp. 303–318, 2017.

[15] Y. Ding and B. D. Rao, "Dictionary learning-based sparse channel representation and estimation for FDD massive MIMO systems," *IEEE Transactions on Wireless Communications*, vol. 17, no. 8, pp. 5437–5451, 2018.

[16] Y. Han, Q. Liu, C. Wen, M. Matthaiou, and X. Ma, "Tracking FDD massive MIMO downlink channels by exploiting delay and angular reciprocity," *IEEE Journal of Selected Topics in Signal Processing*, vol. 13, no. 5, pp. 1062–1076, 2019.

[17] A. Adhikary, E. Al Safadi, M. K. Samimi, R. Wang, G. Caire, T. S. Rappaport, and A. F. Molisch, "Joint spatial division and multiplexing for mm-Wave channels," *IEEE Journal on Selected Areas in Communications*, vol. 32, no. 6, pp. 1239–1255, 2014.

[18] Y. Zeng and R. Zhang, "Millimeter wave MIMO with lens antenna array: A new path division multiplexing paradigm," *IEEE Transactions on Communications*, vol. 64, no. 4, pp. 1557–1571, 2016.

[19] L. You, X. Gao, G. Y. Li, X.-G. Xia, and N. Ma, "BDMA for millimeter-wave/terahertz massive MIMO transmission with per-beam synchronization," *IEEE Journal on Selected Areas in Communications*, vol. 35, no. 7, pp. 1550–1563, 2017.

[20] M. B. Khalilsarai, S. Haghighatshoar, X. Yi, and G. Caire, "FDD massive MIMO via UL/DL channel covariance extrapolation and active channel sparsification," *IEEE Transactions on Wireless Communications*, vol. 18, no. 1, pp. 121–135, 2018.

[21] M. B. Khalilsarai, T. Yang, S. Haghighatshoar, X. Yi, and G. Caire, "Dual-polarized FDD massive MIMO: A comprehensive framework," *arXiv preprint arXiv:2008.11182*, 2020.

[22] R. R. Müller, L. Cottatellucci, and M. Vehkaperä, "Blind pilot decontamination," *IEEE Journal of Selected Topics in Signal Processing*, vol. 8, no. 5, pp. 773–786, 2014.

[23] H. Yin, L. Cottatellucci, D. Gesbert, R. R. Müller, and G. He, "Robust pilot decontamination based on joint angle and power domain discrimination," *IEEE Transactions on Signal Processing*, vol. 64, no. 11, pp. 2990–3003, 2016.
[24] D. Fan, F. Gao, G. Wang, Z. Zhong, and A. Nallanathan, "Angle domain signal processing-aided channel estimation for indoor 60-GHz TDD/FDD massive MIMO systems," *IEEE Journal on Selected Areas in Communications*, vol. 35, no. 9, pp. 1948–1961, 2017.
[25] 3GPP, "Study on 3D channel model for LTE," *Technical Report 3GPP 36.873(V12.7.0)*, 2018.
[26] C. Qian, X. Fu, and N. D. Sidiropoulos, "Algebraic channel estimation algorithms for FDD massive MIMO systems," *IEEE Journal of Selected Topics in Signal Processing*, vol. 13, no. 5, pp. 961–973, 2019.
[27] A. Lu, X. Gao, X. Meng, and X. Xia, "Omnidirectional precoding for 3D massive MIMO with uniform planar arrays," *IEEE Transactions on Wireless Communications*, vol. 19, no. 4, pp. 2628–2642, 2020.
[28] K. Deb, *Multi-Objective Optimization using Evolutionary Algorithms*. John Wiley & Sons, 2001, vol. 16.
[29] J. A. Bondy, U. S. R. Murty *et al.*, *Graph Theory with Applications*. Macmillan London, 1976, vol. 290.
[30] C. A. Sugar and G. M. James, "Finding the number of clusters in a dataset: An information-theoretic approach," *Journal of the American Statistical Association*, vol. 98, no. 463, pp. 750–763, 2003.
[31] P. A. Voois, "A theorem on the asymptotic eigenvalue distribution of Toeplitz-block-Toeplitz matrices," *IEEE Transactions on Signal Processing*, vol. 44, no. 7, pp. 1837–1841, July 1996.
[32] J. Gutiérrez-Gutiérrez, P. M. Crespo *et al.*, "Block Toeplitz matrices: Asymptotic results and applications," *Foundations and Trends® in Communications and Information Theory*, vol. 8, no. 3, pp. 179–257, 2012.

Han Yu (Student Member, IEEE) received the B.E. degree in communication engineering from the Southwest University in 2017. She is currently a Ph.D student at the Department of Electrical Engineering and Electronics, University of Liverpool, U.K. Her current research interests include information theory, graph theory, machine learning, and their applications in wireless communications.

Li You (Member, IEEE) received the B.E. and M.E. degrees from the Nanjing University of Aeronautics and Astronautics, Nanjing, China, in 2009 and 2012, respectively, and the Ph.D. degree from Southeast University, Nanjing, in 2016, all in electrical engineering.

From 2014 to 2015, he conducted Visiting Research at the Center for Pervasive Communications and Computing, University of California Irvine, Irvine, CA, USA. Since 2016, he has been with the Faculty of the National Mobile Communications Research Laboratory, Southeast University. His research interests lie in the general areas of communications, signal processing, and information theory with the current emphasis on massive MIMO communications.

Wenjin Wang (Member, IEEE) received the Ph.D. degree in communication and information systems from Southeast University, Nanjing, China, in 2011. He is currently an Associate Professor with the National Mobile Communications Research Laboratory, Southeast University, Nanjing, China. From 2010 to 2014, he was with the School of System Engineering, University of Reading, Reading, U.K. His research interests include advanced signal processing for future wireless communications and satellite communications. Dr. Wang was awarded a Best Paper Award at IEEE WCSP'09. He was also awarded the first grade Technological Invention Award of the State Education Ministry of China in 2009.

Xinping Yi (Member, IEEE) received the Ph.D. degree in electronics and communications from Télécom ParisTech, Paris, France, in 2015. He is currently a Lecturer (Assistant Professor) with the Department of Electrical Engineering and Electronics, University of Liverpool, U.K. Prior to Liverpool, he was a Research Associate with Technische Universität Berlin, Berlin, Germany, from 2014 to 2017, a Research Assistant with EURECOM, Sophia Antipolis, France, from 2011 to 2014, and a Research Engineer with Huawei Technologies, Shenzhen, China, from 2009 to 2011. His main research interests include information theory, graph theory, and machine learning, and their applications in wireless communications and artificial intelligence.